Article

Molecular Cell

Histone H2AK119 Mono-Ubiquitination Is Essential for Polycomb-Mediated Transcriptional Repression

Graphical Abstract

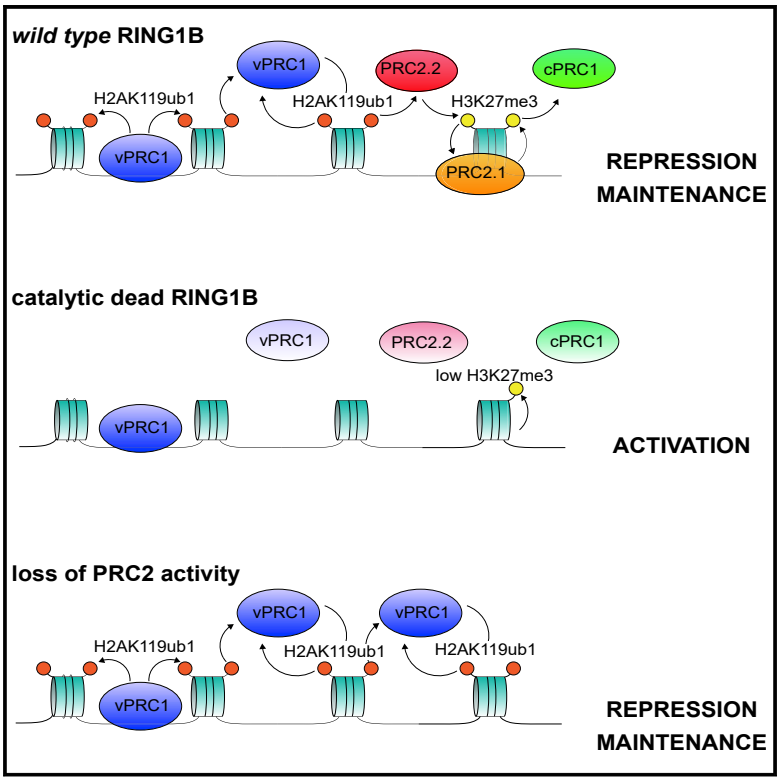

Highlights

- Catalytic inactive RING1B I53S leads to complete loss of H2AK119ub1 deposition
- H2AK119ub1 is essential for the transcriptional repression of all RING1A/B targets
- H2AK119ub1 stabilizes cPRC1 and PRC2 activities, promoting H3K27me3 deposition
- Chromatin binding of variant PRC2.2 is preferentially impaired by loss of H2AK119ub1

Authors

Simone Tamburri, Elisa Lavarone, Daniel Fernández-Pérez, Eric Conway, Marika Zanotti, Daria Manganaro, Diego Pasini

Correspondence

diego.pasini@ieo.it

In Brief

H2AK119ub1 deposition acts as a central hub for mounting PcG repressive machineries. Tamburri et al. dissected the role of H2AK119ub1 in stabilizing PRC2 and canonical PRC1 activities, highlighting how the deposition of H2AK119ub1, but not the structural assembly of PRC1 complexes, is essential to maintain transcriptional repression.

Tamburri et al., 2020, Molecular Cell 77, 840–856
February 20, 2020
https://doi.org/10.1016/j.molcel.2019.11.021

CellPress

CellPress

Molecular Cell
Article

Histone H2AK119 Mono-Ubiquitination Is Essential for Polycomb-Mediated Transcriptional Repression

Simone Tamburri,[1,3] Elisa Lavarone,[1,3] Daniel Fernández-Pérez,[1,2] Eric Conway,[1] Marika Zanotti,[1] Daria Manganaro,[1] and Diego Pasini[1,2,4,*]

[1]Department of Experimental Oncology, IEO European Institute of Oncology IRCCS, Via Adamello 16, 20139 Milan, Italy
[2]Department of Health Sciences, University of Milan, Via A. di Rudinì 8, 20142 Milan, Italy
[3]These authors contributed equally
[4]Lead Contact
*Correspondence: diego.pasini@ieo.it
https://doi.org/10.1016/j.molcel.2019.11.021

SUMMARY

Polycomb group proteins (PcGs) maintain transcriptional repression to preserve cellular identity in two distinct repressive complexes, PRC1 and PRC2, that modify histones by depositing H2AK119ub1 and H3K27me3, respectively. PRC1 and PRC2 exist in different variants and show a complex regulatory cross-talk. However, the contribution that H2AK119ub1 plays in mediating PcG repressive functions remains largely controversial. Using a fully catalytic inactive RING1B mutant, we demonstrated that H2AK119ub1 deposition is essential to maintain PcG-target gene repression in embryonic stem cells (ESCs). Loss of H2AK119ub1 induced a rapid displacement of PRC2 activity and a loss of H3K27me3 deposition. This preferentially affected PRC2.2 variant with respect to PRC2.1, destabilizing canonical PRC1 activity. Finally, we found that variant PRC1 forms can sense H2AK119ub1 deposition, which contributes to their stabilization specifically at sites where this modification is highly enriched. Overall, our data place H2AK119ub1 deposition as a central hub that mounts PcG repressive machineries to preserve cell transcriptional identity.

INTRODUCTION

Organism development and adult tissue homeostasis requires a precise and dynamic control of cellular transcriptional identity. Several chromatin remodeling activities contribute to the establishment of precise transcriptional states by modifying the chromatin environment. This also involves the regulation of post-translational modifications of histone proteins by highly specialized enzymes that by "writing," "reading," and "erasing" specific modifications define the transcriptional state of target genes (Jenuwein and Allis, 2001; Pasini et al., 2008). Consistent with their essential role in controlling cellular identity, these mechanisms also play critical roles in the development of different human pathologies, with cancer being a leading example. Indeed, chromatin modifiers represent one of the most frequently mutated group of genes across all types of human tumors (Comet et al., 2016; Flavahan et al., 2017; Pasini and Di Croce, 2016).

Polycomb group proteins (PcGs) play a central role in these processes and represent the major repressive mechanism utilized in facultative heterochromatin (Bracken and Helin, 2009; Scelfo et al., 2015). PcGs were first discovered in *Drosophila melanogaster* where they play an essential role in maintaining the correct spatiotemporal repression of homeotic genes during fly development (Paro, 1990). This repressive function has been maintained in mammals where PcGs contribute to the repression of all CpG island (CpGi)-containing promoters (Mendenhall et al., 2010; Riising et al., 2014). This involves the cooperative activity of two large polycomb-repressive complexes termed PRC1 and PRC2. Both complexes are characterized by an enzymatic core and by several ancillary subunits that increase biochemical heterogeneity and determine specific biological functions (Chan and Morey, 2019; Margueron and Reinberg, 2011; Pasini and Di Croce, 2016). The PRC1 core is formed by the E3 ligases RING1A or RING1B that, by interacting with the products of one of the six *Pcgf* paralog genes (PCGF1-6), catalyze the mono-ubiquitination of histone H2A at lysine 119 (H2AK119ub1) (Blackledge et al., 2014; Gao et al., 2012; Wang et al., 2004). The PRC2 core is composed by two mutually exclusive methyltransferases, EZH1 and EZH2, that, by associating to the scaffold proteins SUZ12 and EED, catalyze mono-, di-, and tri-methylation of histone H3 lysine 27 (H3K27me1, H3K27me2, and H3K27me3) (Ferrari et al., 2014; Lavarone et al., 2019; Margueron et al., 2008; Shen et al., 2008). Both H2AK119ub1 and H3K27me3 are specifically enriched at repressed CpGi-containing promoters, and their loss correlates with increased transcriptional activity of target genes. The absence of either PRC1 or PRC2 activity results in developmental failure at pre- and post-implantation stages, respectively (Faust et al., 1998; O'Carroll et al., 2001; Pasini et al., 2007; Posfai et al., 2012). In contrast, PRC1 loss of function in adult tissue severely compromises homeostasis that is not phenocopied by loss of PRC2 (Chiacchiera and Pasini, 2017).

The presence of several ancillary subunits determines the existence of many different PRC1 and PRC2 sub-complexes that may confer specific molecular properties and biological functions. PRC2 exists in two major forms: PRC2.1 and PRC2.2. PRC2.1 is characterized by the presence of polycomb-like

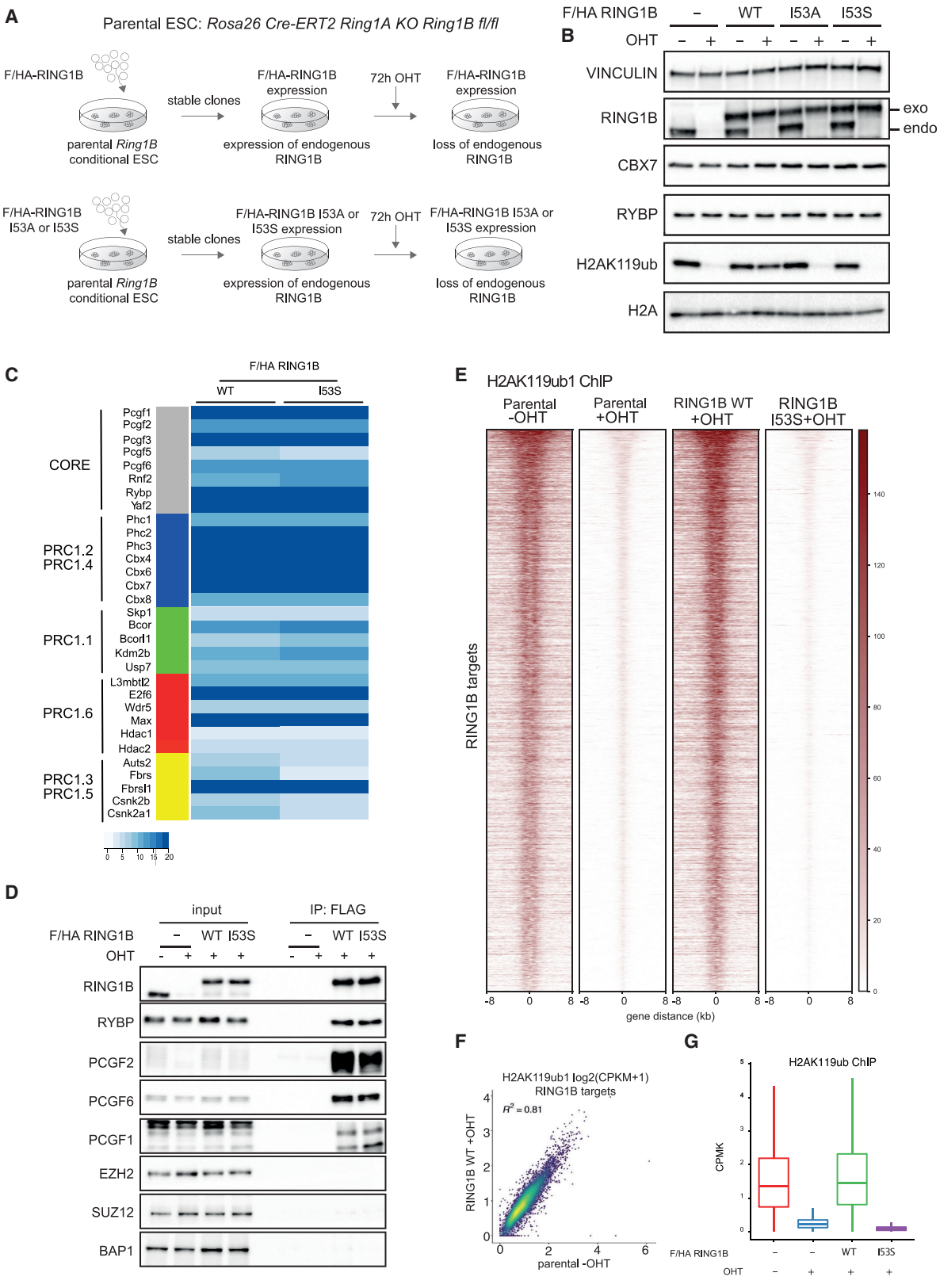

(legend on next page)

subunits (PHF1, MTF2, and PHF19) that confer affinity of the complex to recognize unmethylated CpG islands, and either EPOP or PALI1 (Beringer et al., 2016; Conway et al., 2018). PRC2.2 is characterized by the AEBP2 and JARID2 subunits, where JARID2 provides affinity to PRC2.2 to bind directly to H2AK119ub1 (Blackledge et al., 2014; Cooper et al., 2016; Kalb et al., 2014). PRC1 can instead exist in six distinct complexes (PRC1.1–PRC1.6) characterized by six mutually exclusive PCGF paralog subunits (PCGF1–PCGF6) (Gao et al., 2012; Hauri et al., 2016). PRC1.2 and PRC1.4 complexes are defined as canonical PRC1 (cPRC1) by the presence of CBX subunits that can bind H3K27me3, implying cPRC1 dependency on PRC2 activity (Blackledge et al., 2014; Cao et al., 2002; Tavares et al., 2012). PRC1.1, PRC1.3, PRC1.5, and the PRC1.6 forms exclude CBX proteins by associating with RYBP (or its paralog YAF2), do not recognize H3K27me3, and their activity is independent of PRC2. These PRC1 forms are defined as variant PRC1 (vPRC1) and are tethered to target loci by intrinsic DNA binding activities. This includes PRC1.1 recognition of unmethylated CpG di-nucleotides by the KDM2B subunit (Farcas et al., 2012); PRC1.6 recognition of E-BOX and E2F DNA elements by the MAX/MGA and E2F6/DP dimers stably associated with the complex (Huang et al., 2018; Scelfo et al., 2019; Stielow et al., 2018); and PRC1.3 (and likely PRC1.5) by the recognition of an E-BOX variant directly bound by the USF1/2 transcription factors that can interact with and recruit the PRC1.3 complex to chromatin (Scelfo et al., 2019). Overall, this involves the cooperative activity of both cPRC1 and vPRC1 forms at repressed sites together with the exclusive presence of vPRC1 forms (PRC1.6 and PRC1.3) at several highly expressed genes. While PcG repressed loci display abundant H2AK119ub1 decoration, active vPRC1 targets are characterized by a low-to-absent H2AK119ub1 deposition (Scelfo et al., 2019).

Although the role of vPRC1 complexes in transcriptional regulation remains unclear, these observations suggest that H2AK119ub1 should play a major role in establishing transcriptional repression. Such a model implies an initial deposition of H2AK119ub1 that enhances PRC2 stability, H3K27me3 deposition, recruitment of cPRC1, and establishment of PcG repressive domains (Blackledge et al., 2015). However, the central role of H2AK119ub1 in establishing PcG-mediated repression remains controversial. While different reports provided evidence that H2AK119ub1 is required for the repression of PcG targets without altering PcG-mediated chromatin higher order structures (Kundu et al., 2017), others have shown that the lack of H2AK119ub1 deposition is dispensable for homeotic gene regulation during *Drosophila melanogaster* development (Pengelly et al., 2015). Similarly, mice bearing an inactive RING1B point mutation (I53A) delayed the embryonic lethality of *Ring1B* knockout (KO) mice from E10.5 to E15.5 (Illingworth et al., 2015).

In human tumors, H2AK119ub1 deposition is enhanced by frequent inactivating mutations of the H2AK119ub1-specific deubiquitinase BAP1 (Carbone et al., 2013). Therefore, defining the central role of H2AK119ub1 in mediating transcriptional repression, and its relationship with PRC2 activity, remains an essential question to be addressed. Here, we have developed an inducible system in mouse embryonic stem cells (ESCs) that allows us to dissect the contribution of H2AK119ub1 in regulating PRC1- and PRC2-mediated repression. Using a RING1B I53S catalytically inactive mutant, we showed that lack of H2AK119ub1 deposition, in the absence of cPRC1 and vPRC1 biochemical disruption, massively induced the transcriptional activation of PcG-repressed targets with minimal indirect effects. Mechanistically, this implied a strong destabilization of PRC2 complex activity that resulted in compromised H3K27me3 deposition that preferentially involved the H2AK119ub1-dependent PRC2.2 form. Finally, reduced H3K27me3 activity induced almost complete cPRC1 displacement from chromatin with minor effects on vPRC1 recruitment. Overall, these results place H2AK119ub1 deposition as the central modification for PcG-mediated control of transcriptional repression.

RESULTS

Expression of RING1B I53S Missense Mutation Preserves PRC1 Assembly but Results in Complete Loss of H2AK119ub1 *In Vivo*

To unravel the contribution of RING1B catalytic activity in PRCs-mediated transcriptional repression, we took advantage of *ROSA26::creERT2 RING1A*$^{-/-}$;*RING1B*$^{fl/fl}$ conditional mouse ESCs (Endoh et al., 2008) and manipulated this line (defined as parental from here on) by integrating a vector that stably expressed a FLAG-HA-tagged version of wild-type mouse RING1B (WT) or the RING1B missense mutations I53A and I53S (Figure 1A). Treatment of these ESCs with 4-hydroxy tamoxifen

Figure 1. RING1B I53S Is Fully Catalytically Dead *In Vivo*

(A) Schematic representation of the strategy used for the generation of *ROSA26::creERT2 RING1A*$^{-/-}$;*RING1B*$^{fl/fl}$ conditional mESCs stably expressing FLAG-HA (F/HA)-tagged RING1B WT or I53A/S.

(B) Western blot analysis with the indicated antibodies of total protein extracts obtained from the specified cell lines upon 72 h of treatment with OHT (+OHT) or EtOH (−OHT). Vinculin and histone H2A were used as loading controls.

(C) Values of the LFQ ratios of the RING1B WT and I53S obtained by tandem mass spectrometry (MS/MS) analyses in the RING1B immuno-purifications (anti-FLAG) from *ROSA26::creERT2 RING1A*$^{-/-}$;*RING1B*$^{fl/fl}$ conditional mESCs stably expressing FLAG-HA (F/HA)-tagged RING1B WT or I53S upon 72 h of treatment with OHT (+OHT).

(D) Co-immunoprecipitation analysis of nuclear extracts derived from FLAG-HA (F/HA)-tagged RING1B WT or I53S expressing cells upon 72 h of treatment with OHT (+OHT) or EtOH (−OHT) using M2 affinity gel beads. FLAG-IPs in parental cells served as a negative control.

(E) Heatmaps representing normalized H2AK119ub1 ChIP-seq intensities ±8 kb around the center of RING1B target loci in the indicated cell lines.

(F) Scatterplot showing the relationship between H2AK119ub1 CPMK levels (counts per million per kilobase) between parental EtOH treated (−OHT) and RING1B WT OHT-treated (+OHT) cells in RING1B target loci. R2 represents the coefficient of determination of linear regression.

(G) Boxplots representing H2AK119ub1 ChIP-seq CPMK levels in the indicated cell lines at RING1B target loci.

See also Figure S1A.

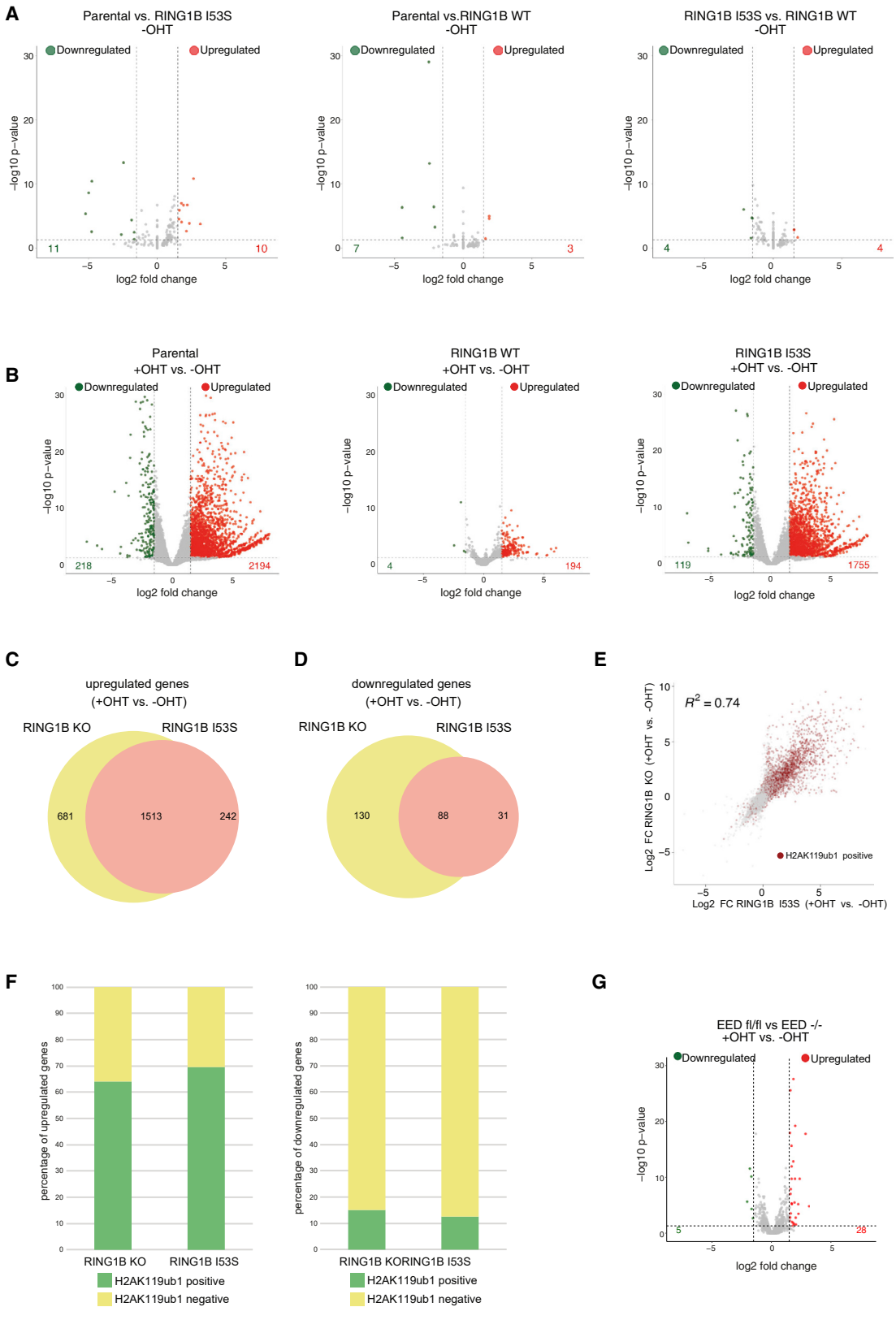

(legend on next page)

(OHT) will induce complete loss of endogenous RING1A/B protein levels in the parental line or leave the unique expression of exogenous RING1B WT or RING1B I53A/S in the engineered ESC clones (Figure 1A). Our previous analysis with this parental line identified that, at 72 h of OHT treatment, endogenous RING1B and H2AK119ub1 deposition were lost (Lavarone et al., 2019). Indeed, at this time point, endogenous RING1B levels were undetectable resulting solely in the expression of the exogenous counterparts (Figure 1B). Importantly, WT and mutant exogenous forms were expressed to the same levels of endogenous RING1B without affecting the expression levels of PRC1 components that define canonical (CBX7) and variant PRC1 forms (RYBP) (Figure 1B). While RING1B WT expression did not alter the overall H2AK119ub1 levels, expression of RING1B I53A and I53S mutants resulted in the global loss of H2AK119ub1 deposition at levels comparable with OHT-treated parental cells (Figure 1B). While the I53A mutation has been previously shown to be hypomorphic with some residual activity of H2AK119ub1 deposition, the I53S was shown to be fully catalytic dead (Ben-Saadon et al., 2006; Buchwald et al., 2006; Elderkin et al., 2007; Illingworth et al., 2015; Tsuboi et al., 2018) as confirmed by the complete lack of H2AK119ub1 deposition observed in our model (Figure 1B). We therefore decided to perform all further molecular analysis with this mutant line. Mass spectrometry analyses and western blot validations of co-immunoprecipitation experiments showed that RING1B I53S efficiently formed canonical and variant PRC1 forms demonstrating that lack of H2AK119ub1 deposition is not a consequence of PRC1 complexes disruption (Figures 1C and 1D; Table S1). Genome-wide localization analyses for H2AK119ub1 extended these observations, demonstrating that RING1B I53S expression induced a complete loss H2AK119ub1 deposition at all PRC1 target loci (Figure 1E; Table S2). Importantly, the expression of RING1B WT perfectly maintained physiological levels of H2AK119ub1 to all target loci (Figures 1E–1G). This result was further validated by chromatin immunoprecipitation (ChIP)-qPCR analyses at selected loci (Figure S1A). Overall, these results demonstrated that the expression of RING1B I53S preserved PRC1 complex formation but was completely catalytically dead *in vivo* at all PRC1 target loci.

Deposition of H2AK119ub1 Is Essential for PRC1-Mediated Transcriptional Repression

Determining whether deposition of H2AK119ub1 is required for PRC1-mediated transcriptional repression remains an important open question. We took advantage of our model system to address this by performing RNA sequencing (RNA-seq) analysis in parental, RING1B WT and RING1B I53S ESCs at 72 h after OHT treatment. Importantly, in the presence of endogenous RING1B expression (vehicle EtOH treatment: −OHT), ectopic expression of RING1B WT or I53S mutant did not alter the transcriptional landscape of ESCs demonstrating that the I53S mutation does not exert any dominant-negative effect on PRC1 activity (Figure 2A). Consistent with the repressive role of PRC1, addition of OHT to parental cells specifically induced the upregulation of a large number of repressed genes (Figure 2B; Table S3). While this effect is rescued by the ectopic expression of RING1B WT, the lack of H2AK119ub1 deposition—induced by RING1B I53S expression—perfectly phenocopied the transcriptional effects induced by global loss of PRC1 activity (Figures 2B and 2C). Few genes were also downregulated in both conditions suggesting common indirect effects (Figure 2D). Correlation plots further demonstrated high transcriptional concordance between parental and I53S ESCs upon OHT treatment (Figure 2E), highlighting how genes enriched for H2AK119ub1 at their promoters are mostly upregulated (Figure 2E, red dots). Indeed, while the vast majority of upregulated genes are targets of PRC1 enzymatic activity, the few downregulated genes were mostly free of H2AK119ub1 deposition (Figure 2F). This was not the consequence of a deregulated PRC2 activity, because its acute inactivation, using *Eed*$^{fl/fl}$ conditional KO ESCs at 72 h of OHT treatment, resulted in a complete loss of H3K27me3 deposition (Figure S1B) but failed to recapitulate the transcriptional defects observed in absence of RING1A/B or H2AK119ub1 (Figure 2G). Overall, these data directly place H2AK119ub1 deposition as an essential modification to maintain transcriptional repression of CpG-rich promoters.

H2AK119ub1 Controls H3K27me3 Deposition by Regulating PRC2 Recruitment

The mechanisms by which H2AK119ub1 could control transcriptional repression are still a matter of debate. H2AK119ub1 could be the end product of a PRC2-PRC1 functional crosstalk (canonical model) or the triggering modification that determines the recruitment of PRC1-PRC2 machineries. Using our system, we demonstrated that loss of H2AK119ub1 did not alter the expression levels of core PRC2 components (EZH2, SUZ12, and EED) as well as of sub-stoichiometric subunits that define the PRC2.1 (MTF2 and EPOP) and PRC2.2 (JARID2 and AEBP2) variants

Figure 2. H2AK119ub1 Is Essential for PRCs-Mediated Transcriptional Repression

(A) Volcano plots of –log10 (p value) against log2 fold change representing the differences in gene expression, related to RNA-seq analysis, in the indicated cell lines upon EtOH treatment (−OHT). Upregulated (red) and downregulated (green) genes are highlighted.

(B) As in (A) upon OHT treatment (+OHT).

(C) Venn diagrams showing the overlap of upregulated genes between the indicated cell lines.

(D) As in (C) for downregulated genes.

(E) Scatterplot showing the relationship between log2 fold changes (FC) between the indicated cell lines at RING1B target loci. R2 represents the coefficient of determination of linear regression. Genes with promoters (±2.5 kb around transcription start site [TSS]) containing H2AK119ub1 peaks are highlighted in red.

(F) Barplots showing the percentage of upregulated (left) or downregulated (right) genes with promoters (±2.5 kb around TSS) containing H2AK119ub1 peaks in the indicated cell lines.

(G) Volcano plots of –log10 (p value) against log2 fold change representing the differences in gene expression, related to RNA-seq analysis, in *EED*$^{fl/fl}$ versus *EED*$^{-/-}$ ESCs. Upregulated (red) and downregulated (green) genes are highlighted.

See also Figure S1B.

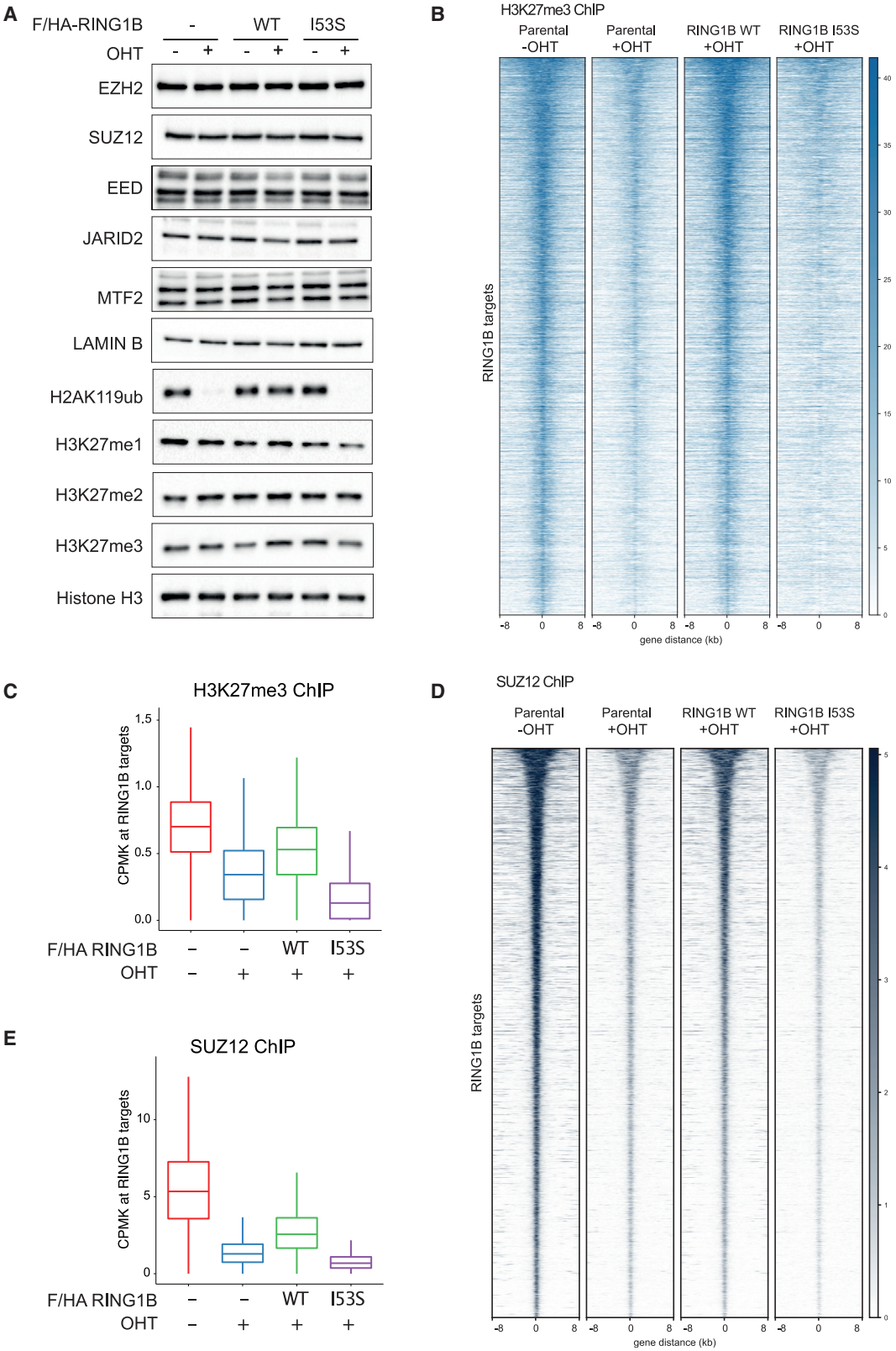

(legend on next page)

(Figures 3A and S1C). Consistent with the role of PcGs in repressing *Aebp2* transcription (Healy et al., 2019), the expression of the short AEBP2 isoform (Grijzenhout et al., 2016) was increased in absence of H2AK119ub1 deposition, while the long AEBP2 isoform levels 2remained constant. We have noticed a modest reduction in H3K27me3 bulk levels in the absence of H2AK119ub1 deposition that suggest reduced PRC2 activity in agreement with previous reports (Blackledge et al., 2014; Fursova et al., 2019; Rose et al., 2016). Indeed, genome-wide mapping of H3K27me3 deposition clearly showed a specific reduction of this modification demonstrating that PRC2 activity is severely affected by loss of H2AK119ub1 deposition (Figures 3B and 3C). This is consistent with the strong displacement of PRC2 from target loci observed by SUZ12 ChIP-seq analyses upon expression of RING1B I53S (+OHT) (Figures 3D and 3E). Overall, these results demonstrate that H2AK119ub1 is required to maintain efficient PRC2 recruitment and activity at its target sites.

H2AK119ub1 Loss Differentially Affects PRC2.1 and PRC2.2 Chromatin Occupancy

The role that H2AK119ub1 plays in the recruitment of PRC2 also remains poorly characterized *in vivo*. Both H3K27me3 and H2AK119ub1 could serve as docking sites to stabilize PRC2 forms at target loci. Biochemical analyses has shown that JARID2 has direct affinity for H2AK119ub1 (Cooper et al., 2016) implying that PRC2.2 should be more dependent on this modification for its association at target promoters. At the same time, H3K27me3 can also serve as an affinity site for both PRC2.1 and PRC2.2 by EED recognition (Margueron et al., 2009). H3K27me3 binding by the WD40 repeats of EED stimulates PRC2 enzymatic activity allosterically inducing H3K27me3 spreading (Lee et al., 2018; Margueron et al., 2009). To shed light into this complex regulatory system, we tested whether loss of H2AK119ub1 deposition preferentially affected PRC2.1 and PRC2.2 target gene association by ChIP-seq analyses for MTF2 and JARID2, respectively. To dissect the kinetics of PRC2 eviction from chromatin, we performed a time course induction of *Ring1B* KO at 24, 48, and 72 h. While at 24 h global PRC1 activity was still not fully depleted, at 48 and 72 h, H2AK119ub1 deposition and RING1B levels were fully lost at a comparable extent (Figures S1D and S1E). ChIP-seq analysis at these time points revealed that both complex variants were affected by loss of H2AK119ub1 deposition (Figures 4A–4D). However, while JARID2 was already fully displaced at 48 h, MTF2 displacement showed a slower kinetic of displacement maintaining significant chromatin occupancy also at 72 h from OHT treatment (Figures 4E and 4F). These data are consistent with a direct role for JARID2 in recruiting PRC2.2 to chromatin via H2AK119ub1 recognition and with the MTF2-containing PRC2.1 form being less sensitive to H2AK119ub1 loss in agreement with recent reports using RING1A/B null ESCs (Healy et al., 2019). To further investigate the differential displacement of PRC2.1 compared to PRC2.2, we performed ChIP-seq analysis for EPOP (PRC2.1) and AEBP2 (PRC2.2) at 72 h of OHT treatment. Consistent with our previous observation, AEBP2 was displaced from chromatin in the absence of H2AK119ub1, while EPOP persisted on chromatin similarly to MTF2 (Figured 4G–4J and S1E). These results demonstrate the central role of H2AK119ub1 in mounting primarily PRC2.2 at promoters while also stabilizing PRC2.1 association. Overall, H2AK119ub1 deposition sustains a positive feedback mechanism that allows the stabilization of PRC2 activities at target promoters.

MTF2 Is Required for Residual PRC2.1 Chromatin Occupancy in the Absence of H2AK119ub1

To further probe the mechanism of PRC2 recruitment in ESCs, we knocked out *Mtf2* in our *Ring1B* conditional KO system (Figure S1F). With this tool, we performed ChIP-seq analysis for H3K27me3 and SUZ12 before and after OHT treatment. In agreement with recent publications (Healy et al., 2019; Hojfeldt et al., 2019), loss of MTF2 in the presence of RING1B expression led to reduced SUZ12 and H3K27me3 levels (Figures 5A–5F). The extent of this reduction is comparable with the reduction of H3K27me3 and SUZ12 observed in absence of RING1B or in absence of H2AK119ub1 deposition in MTF2-proficient ESCs. Importantly, combining MTF2 KO either with RING1B loss or in absence of H2AK119ub1, resulted in an almost complete displacement of SUZ12 from target loci and global lack of H3K27me3 deposition (Figures 5A–5F). Overall, these data demonstrate that, although loss of H2AK119ub1 can destabilize PRC2.1 activity, its ground-state association with target loci remains independent of H2AK119ub1 to sustain significant H3K27me3 deposition.

H2AK119ub1 Deposition Affects General RING1B Stability at Target Loci

The largest fraction of RING1B associated at target loci is dependent on H3K27me3 deposition. Only a minor residual fraction, corresponding to ~10% of RING1B signal, does not depend on this modification. However, this residual amount is highly active and is sufficient to preserve normal H2AK119ub1 deposition (Blackledge et al., 2014; Tavares et al., 2012). We therefore tested whether H2AK119ub1-dependent loss of H3K27me3 affected RING1B chromatin association. As expected, the vast majority of RING1B was displaced from target loci, both in parental and RING1B I53S ESCs treated with OHT (Figures 6A and 6B). This is not an intrinsic defect of the RING1B I53S mutant: RING1B I53S can assemble as a part of normal PRC1 complexes (Figures

Figure 3. H2AK119ub1 Deposition Is Required for PRC2 Recruitment and Activity

(A) Western blot analysis with the indicated antibodies of protein extracts obtained from the specified cell lines upon 72 h of treatment with OHT (+OHT) or EtOH (−OHT). LAMIN B and histone H3 were used as loading controls.

(B) Heatmaps representing normalized H3K27me3 ChIP-seq intensities ±8 kb around the center of RING1B target loci in the indicated cell lines.

(C) Boxplots representing H3K27me3 ChIP-seq CPMK levels in the indicated cell lines at RING1B target loci.

(D) Heatmaps representing normalized SUZ12 ChIP-seq intensities ±8 kb around the center of RING1B target loci in the indicated cell lines.

(E) Boxplots representing SUZ12 ChIP-seq CPMK levels in the indicated cell lines at RING1B target loci.

See also Figure S1C.

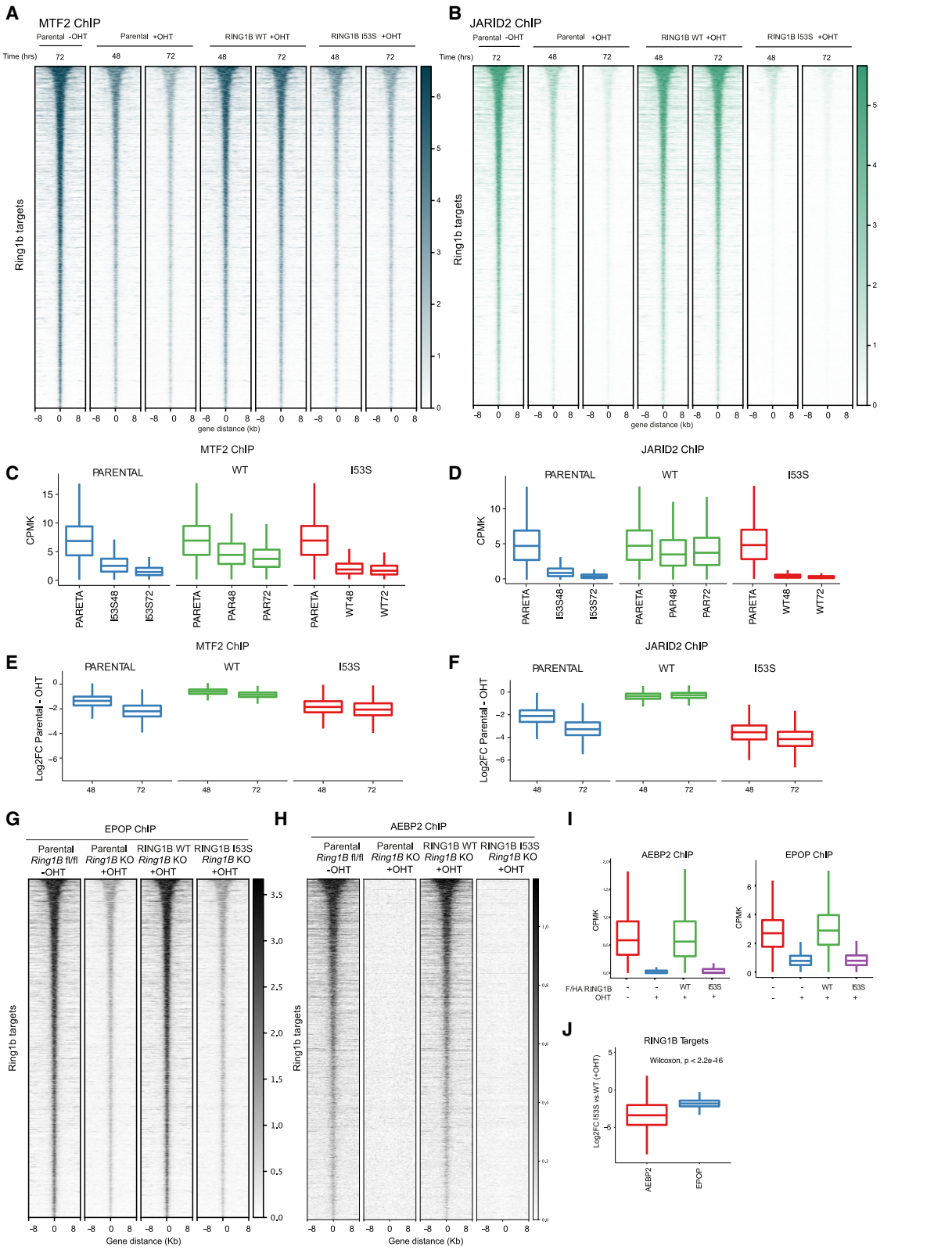

(legend on next page)

1C and 1D) and can be efficiently recruited to target loci when H2AK119ub1 deposition is present (Figure 6C). Additionally, RING1B I53S fractionated in the nuclear insoluble fraction with the same efficiency of RING1B WT (Figure 6D). This demonstrated that neither localization nor chemical properties are altered by the mutation. This suggests that RING1B I53S displacement from target loci is a secondary effect of H2AK119ub1 and H3K27me3 loss. Indeed, RING1B was also globally displaced to a similar extent in EZH1/2 double KO ESCs (Figures 6E and 6F), which lack H3K27me3 deposition but retain normal H2AK119ub1 levels (Lavarone et al., 2019). Overall, these results suggest that lack of H2AK119ub1 triggers a secondary displacement of the PRC1 complex from target loci that could depend on impaired PRC2 localization.

H2AK119ub1 Loss Preferentially Affects cPRC1 versus vPRC1

Chromatin association of cPRC1 has been extensively described to depend on H3K27me3 deposition (Scelfo et al., 2015). This affinity is conferred by the chromodomain of CBX proteins that are not present in vPRC1 forms (Bernstein et al., 2006; Cao et al., 2002). Indeed, RING1B residual binding in *Eed* KO ESCs was shown to depend on vPRC1 forms compared to cPRC1 (Tavares et al., 2012). We therefore tested if cPRC1 binding is specifically affected in the absence of H2AK119ub1 deposition by analyzing PCGF2 and CBX7 (cPRC1) compared to PCGF6 and RYBP (vPRC1) behavior. PCGF2 levels were destabilized in the absence of endogenous RING1B expression in agreement with previous reports (Scelfo et al., 2019) (Figure S2A). Importantly, RING1B WT and I53S rescued PCGF2 degradation to a similar extent, confirming that complex assembly—but not activity—is required for PCGF2 stability (Figure S2A). At the genome-wide level, PCGF2 and CBX7 association at target loci was preserved by the expression of RING1B WT but was strongly compromised by the absence of H2AK119ub1 deposition (Figures 7A and 7B). This is consistent with the reduced H3K27me3 levels observed in the absence of H2AK119ub1 deposition (Figures 3B and 3C). Unexpectedly, PCGF6 and RYBP binding was also affected by the loss of H2AK119ub1, however, to a much lower extent than PCGF2 and CBX7 (Figures 7C–7E). Importantly, we have previously shown that, while PCGF6 (PRC1.6) associates to a large set of target promoters together with PRC1.2 and PRC1.1, it also shares a substantial set of unique target sites with lower levels of H2AK119ub1 (Scelfo et al., 2019). To gain further insights related to the role that H2AK119ub1 plays in stabilizing PRC1.6 binding at target loci, we stratified PCGF6 targets based on the occupancy of PCGF proteins (Scelfo et al., 2019). Such analysis highlighted that, while PCGF6 binding was affected at sites that are co-occupied with PCGF2 and presented higher levels of H2AK119ub1 and H3K27me3 deposition, its binding at unique targets was not affected by loss of H2AK119ub1 deposition (Figures 7F and S2B). Similar to PRC2.2, vPRC1 also have an affinity for H2AK119ub1 (Kalb et al., 2014). This was further supported by CBX7 displacement at PCGF2-occupied sites and by the retention of RYPB binding at unique sites (Figures 7G and S2C). Overall, our results demonstrate that, while cPRC1 association is highly dependent on H2AK119ub1 deposition, vPRC1 target association can be stabilized by the high H2AK119ub1 levels found at repressed sites but retain intrinsic independent affinities for its target loci.

DISCUSSION

The molecular mechanisms by which PRC1 and PRC2 activities control gene repression largely remain a matter of debate (Chan and Morey, 2019; Pasini and Di Croce, 2016). In this context, the role of cPRC1 versus vPRC1 activity in mediating gene repression, as well as the direct role that H2AK119ub1 plays in this context, is an important open issue that requires further investigation. Here, we have developed a simple model that generates inducible expression of a fully catalytically inactive form of RING1B (RING1B I53S in a RING1A null background) to dissect the contribution of H2AK119ub1 deposition to the structural properties of PRC1. This system allows monitoring of the acute effects induced by the loss of H2AK119ub1 deposition by preventing transcriptional adaptations and indirect effects that occur in constitutive PcG mutant ESCs maintained in pluripotent conditions (Fursova et al., 2019; Scelfo et al., 2019). With this system, we showed that the expression of the catalytic inactive RING1B I53S neither affected the assembly of distinct PRC1 sub-complexes (Table S1), nor its ability to associate with target promoters (Table S2), but it did fail to maintain transcriptional repression of target genes to an identical extent as global RING1A/B deletion including the Hox clusters (Table S3).

Figure 4. H2AK119ub1 Loss Preferentially Abolishes PRC2.2 while Reducing PRC2.1 Chromatin Occupancy

(A) Heatmaps representing normalized MTF2 ChIP-seq intensities ±8 kb around the center of RING1B target loci in the indicated cell lines at the indicated time point post OHT induction.

(B) Heatmaps representing normalized JARID2 ChIP-seq intensities ±8 kb around the center of RING1B target loci in the indicated cell lines at the indicated time point post OHT induction.

(C) Boxplot representing MTF2 ChIP-seq CPMK levels in the indicated cell lines at RING1B target loci at the indicated time point post OHT induction.

(D) Boxplot representing JARID2 ChIP-seq CPMK levels in the indicated cell lines at RING1B target loci at the indicated time point post OHT induction.

(E) Boxplot representing the log2 ratio of MTF2 CPMK levels at RING1B target loci between RING1B WT- and I53S-expressing cells at the indicated time point post OHT induction.

(F) Boxplot representing the log2 ratio of JARID2 CPMK levels at RING1B target loci between RING1B WT- and I53S-expressing cells at the indicated time point post OHT induction.

(G) Heatmaps representing normalized EPOP ChIP-seq intensities ±8 kb around the center of RING1B target loci in the indicated cell lines.

(H) Heatmaps representing normalized AEBP2 ChIP-seq intensities ±8 kb around the center of RING1B target loci in the indicated cell lines.

(I) Boxplot representing AEBP2 (left) or EPOP (right) ChIP-seq CPMK levels in the indicated cell lines at RING1B target loci.

(J) Boxplot representing the log2 ratio of AEBP2 or EPOP CPMK levels at RING1B target loci between RING1B WT- and I53S-expressing cells.

See also Figures S1D and S1E.

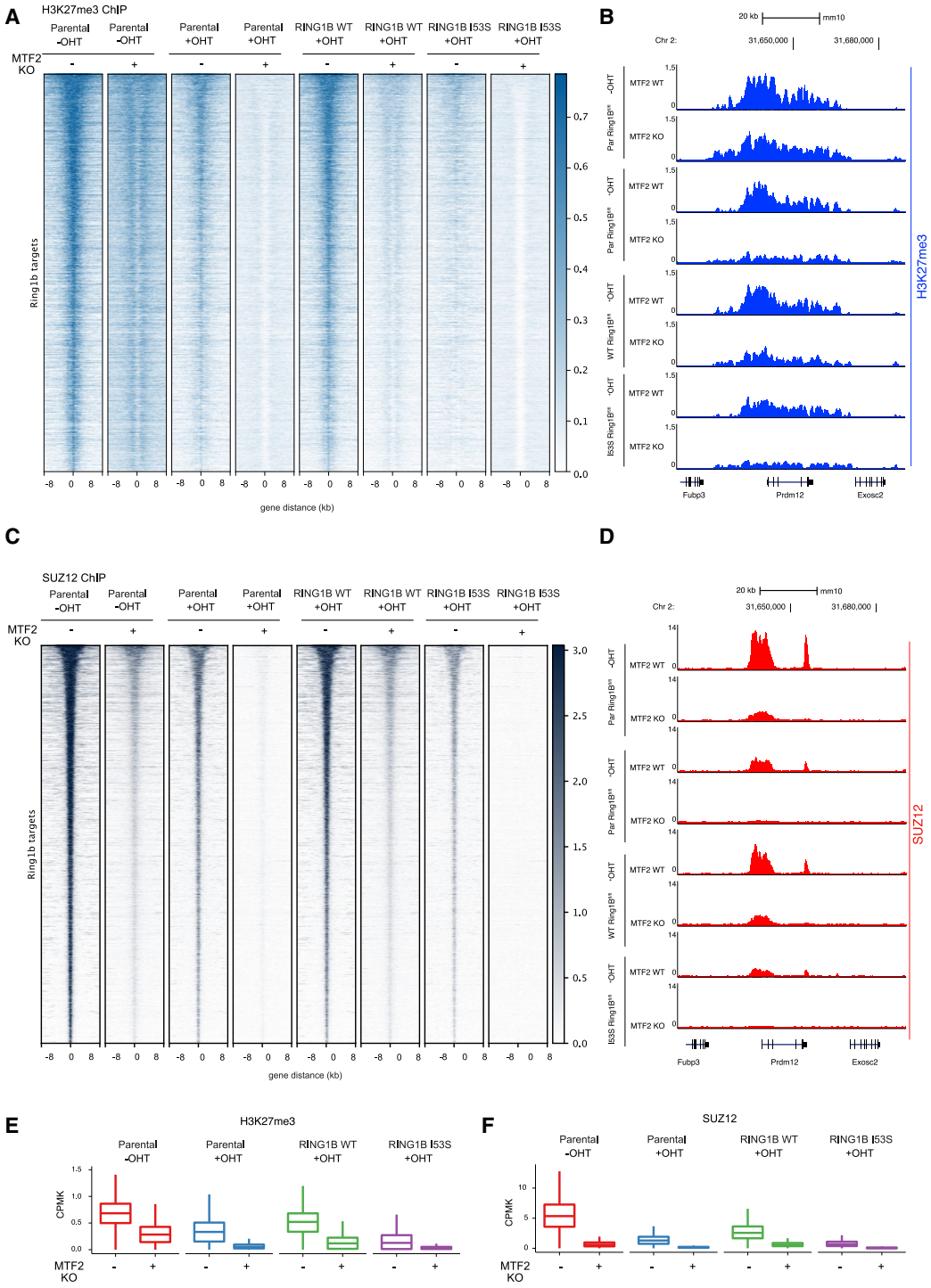

Figure 5. MTF2 Is Responsible for Residual PRC2 Binding upon H2AK119ub1 Loss

(A) Heatmaps representing normalized H3K27me3 ChIP-seq intensities ±8 kb around the center of RING1B target loci in the indicated cell lines.

(B) Representative genomic snapshots of H3K27me3 ChIP tracks at the PRDM12 gene locus.

(C) Heatmaps representing normalized SUZ12 ChIP-seq intensities ±8 kb around the center of RING1B target loci in the indicated cell lines.

(D) Representative genomic snapshots of SUZ12 ChIP tracks at the PRDM12 gene locus.

(E) Boxplot representing H327me3 ChIP-seq CPMK levels in the indicated cell lines at RING1B target loci.

(F) Boxplot representing SUZ12 ChIP-seq CPMK levels in the indicated cell lines at RING1B target loci.

See also Figure S1F.

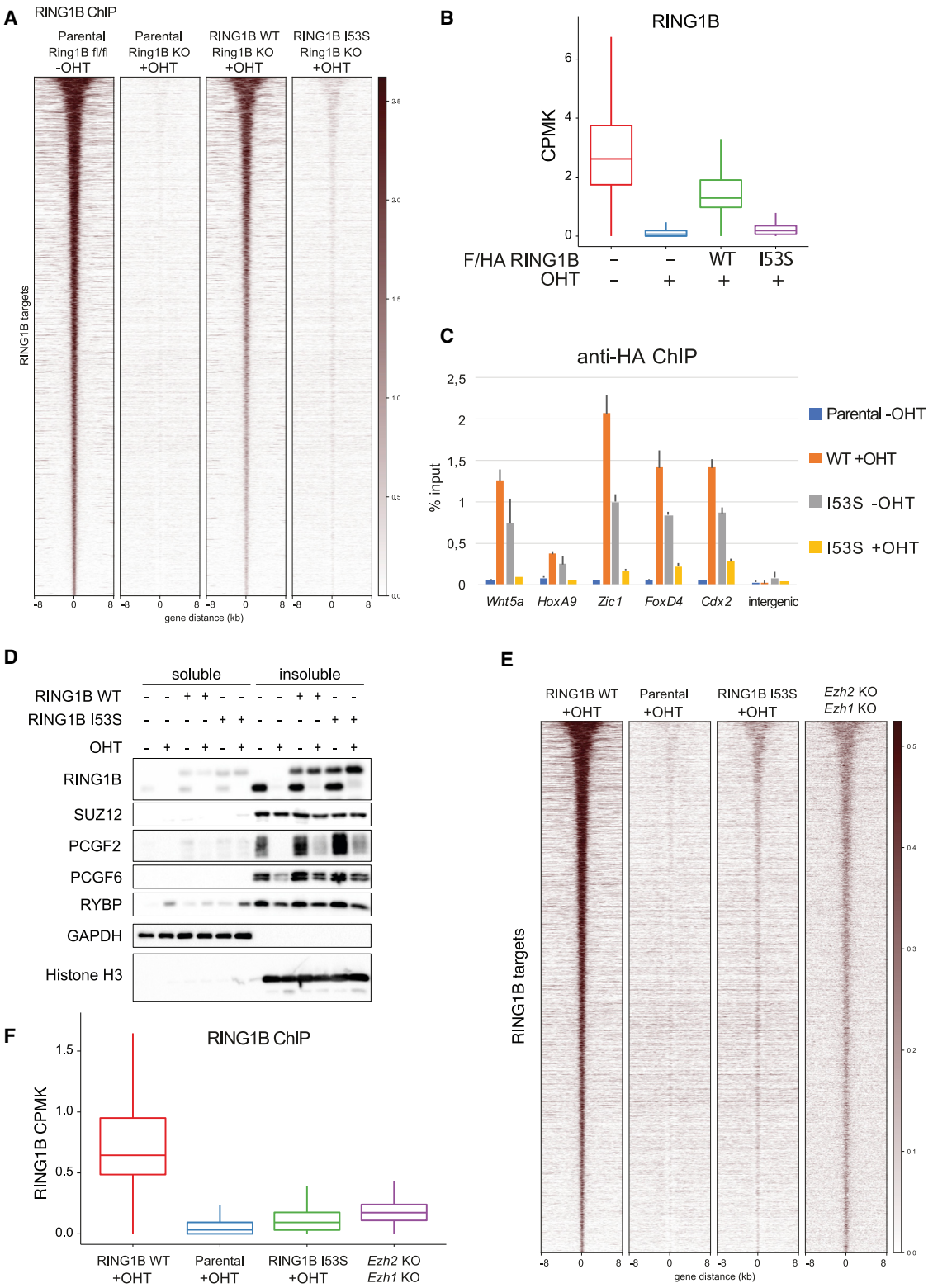

Figure 6. H2AK119ub1 Affects RIN1GB Chromatin Stability

(A) Heatmaps representing normalized RING1B ChIP-seq intensities ±8 kb around the center of RING1B target loci in the indicated cell lines.

(B) Boxplots representing RING1B ChIP-seq CPMK levels in the indicated cell lines at RING1B target loci.

(C) ChIP-qPCR analysis of HA in the indicated cell lines at five specific polycomb targets and one intergenic region. Parental cells served as a negative control.

(legend continued on next page)

Importantly, loss of EED at the same time point did not induce large-scale transcriptional changes in agreement with previous reports using an RNA interference approach (Riising et al., 2014). In fact, very few genes were upregulated in these conditions, demonstrating that H2AK119ub1 deposition is sufficient to maintain full transcriptional repression in the absence of global PRC2 activity. This demonstrates the essential role of H2AK119ub1 deposition in maintaining transcriptional repression at genome-wide levels in agreement with previous reports that analyzed selected target genes (Endoh et al., 2012). However, this differs from the role that was proposed for H2AK118ub1 (K119 in vertebrates) in *Drosophila melanogaster*. In this organism, H2AK118ub1 deposition was not required for correct spatiotemporal expression of homeotic genes during development (Pengelly et al., 2015) in contrast to the essential role played by H3K27me3 in the same context (Pengelly et al., 2013). Although PRC2 recognition of H2AK118ub1 is conserved in flies, these results suggest that loss of H2AK118ub1 is not sufficient to affect PRC2 activity at homeotic genes, perhaps due to the redundant functions between PRC2.2 and PRC2.1, which is less affected by H2AK119ub1 loss. This is in line with the report that constitutive RING1B I53A mutant mice showed a substantial delay in embryonic lethality in contrast to *Ring1B* KOs (from E10.5 to E15.5) (Illingworth et al., 2015). Nonetheless, it remains unclear to what extent this developmental delay is directly caused by the lack of maintenance of target gene repression. Moreover, the hypomorphic properties of the RING1B I53A mutant (Tsuboi et al., 2018) used in this study, coupled to the expression of a proficient *Ring1A* allele, did not rule out the central role of H2AK119ub1 deposition in controlling transcriptional repression and early development. Now, our data have demonstrated the essential contribution of H2AK119ub1 deposition in PcG-mediated transcriptional repression, including HOX genes clusters. The different modalities of PcG complexes recruitment, together with the increased biochemical complexity of vPRC1 activity between flies and mammals, allows us to speculate that during vertebrate evolution a central role for H2AK119ub1 deposition in PcG-mediated transcriptional repression arose. The generation of more sophisticated and precise mouse models will become essential to dissect the contribution of H2AK119ub1-mediated control of transcriptional repression with respect to the more general role of PRC1 activities in development.

The work of several laboratories including ours have also highlighted that mammalian PRC1 exist in distinct biochemical forms (Gao et al., 2012) that are not exclusively associated with transcriptional repression (Fursova et al., 2019; Scelfo et al., 2019). Actively transcribed sites are specifically associated with PRC1.1, PRC1.3, or PRC1.6 forms. However, in this context, the role of H2AK119ub1 seems to be marginal as the vPRC1 forms associated with transcribed loci displayed low-to-absent H2AK119ub1 levels (Pivetti et al., 2019; Scelfo et al., 2019). The contribution of these PRC1 forms to active transcription remains poorly understood, but is possible that these properties could have specific developmental roles that are not linked to H2AK119ub1 deposition and gene repression. Further studies in this direction are needed to dissect the repressive versus the potential activatory role of specific vPRC1 forms. Our new data make a large step in this direction demonstrating that, in the context of PcG-mediated transcriptional repression of CpGi containing promoters, H2AK119ub1 deposition serves as a central hub to maintain proper repression of target genes.

How PcGs establish and maintain transcriptional repression is also a matter of debate. Whether PRC2 controls PRC1 recruitment (canonical model) or PRC1 controls PRC2 (variant or non-canonical model) remains an open discussion (Chan and Morey, 2019; Pasini and Di Croce, 2016). Our data clearly show that H2AK119ub1 functions as a "glue" that keeps PRC1 and PRC2 machineries tethered to repressed loci at a genome-wide scale. Loss of H2AK119ub1 destabilizes PRC2 recruitment and H3K27me3 deposition, which induces displacement of cPRC1 forms, disrupting proper PcG repressive domains. The finding that this rapidly and preferentially affected PRC2.2 activity is in agreement with the specific affinity of JARID2 for H2AK119ub1 (Cooper et al., 2016; Kalb et al., 2014). Our evidence for redundant recruitment mechanisms for the distinct PRC2 sub-complexes is in line with recent reports (Healy et al., 2019; Laugesen et al., 2019). Nonetheless, PRC2.1 was also affected in the absence of H2AK119ub1, suggesting a complex interplay between PRC2 variants. This could be an indirect consequence of reduced deposition of H3K27me3 levels together with a reduced affinity of PRC2.1 for target genes that is consistent with the mild impairment of MTF2 chromatin occupancy observed in *Jarid2* KO ESCs (Healy et al., 2019). Low H3K27me3 levels could reduce EED affinity for its target sites, compromising spreading and establishment of PcG domains (Lee et al., 2018; Oksuz et al., 2018). Reduced H3K27me3 deposition further correlated with specific cPRC1 displacement from all repressed target loci (represented by PCGF2 and CBX7 ChIP-seq), in agreement with cPRC1 being dependent on the deposition of this modification through the specific activity of CBX proteins (Bernstein et al., 2006; Cao et al., 2002). CBXs are excluded from vPRC1 forms by RYBP that were indeed less affected by lack of H2AK119ub1 deposition (exemplified by PCGF6 and RYBP ChIP-seq). These results agree with the existence of distinct and specific mechanisms by which cPRC1 versus vPRC1 forms are recruited to DNA and place vPRC1 activities upstream to cPRC1.

Our data also showed that RING1B I53S becomes strongly destabilized from target genes in the absence of H2AK119ub1. This was primarily a consequence of the specific displacement of cPRC1 as a similar RING1B displacement was observed upon inactivation of PRC2 activity or upon expression of a catalytic-inactive PRC2 mutant that lack H3K27me3 deposition in the presence of normal H2AK119ub1 levels (Lavarone et al., 2019; Tavares et al., 2012). Indeed, significant binding of vPRC1 was

(D) Western blot analysis with the indicated antibodies of soluble and insoluble protein fractions obtained from the specified cell lines upon 72 h of treatment with OHT (+OHT) or EtOH (−OHT). GAPDH and histone H3 were used as positive controls for the soluble and insoluble fractions, respectively.
(E) Heatmaps representing normalized RING1B ChIP-seq intensities ±8 kb around the center of RING1B target loci in the indicated cell lines.
(F) Boxplots representing RING1B ChIP-seq CPMK levels in the indicated cell lines at RING1B target loci.

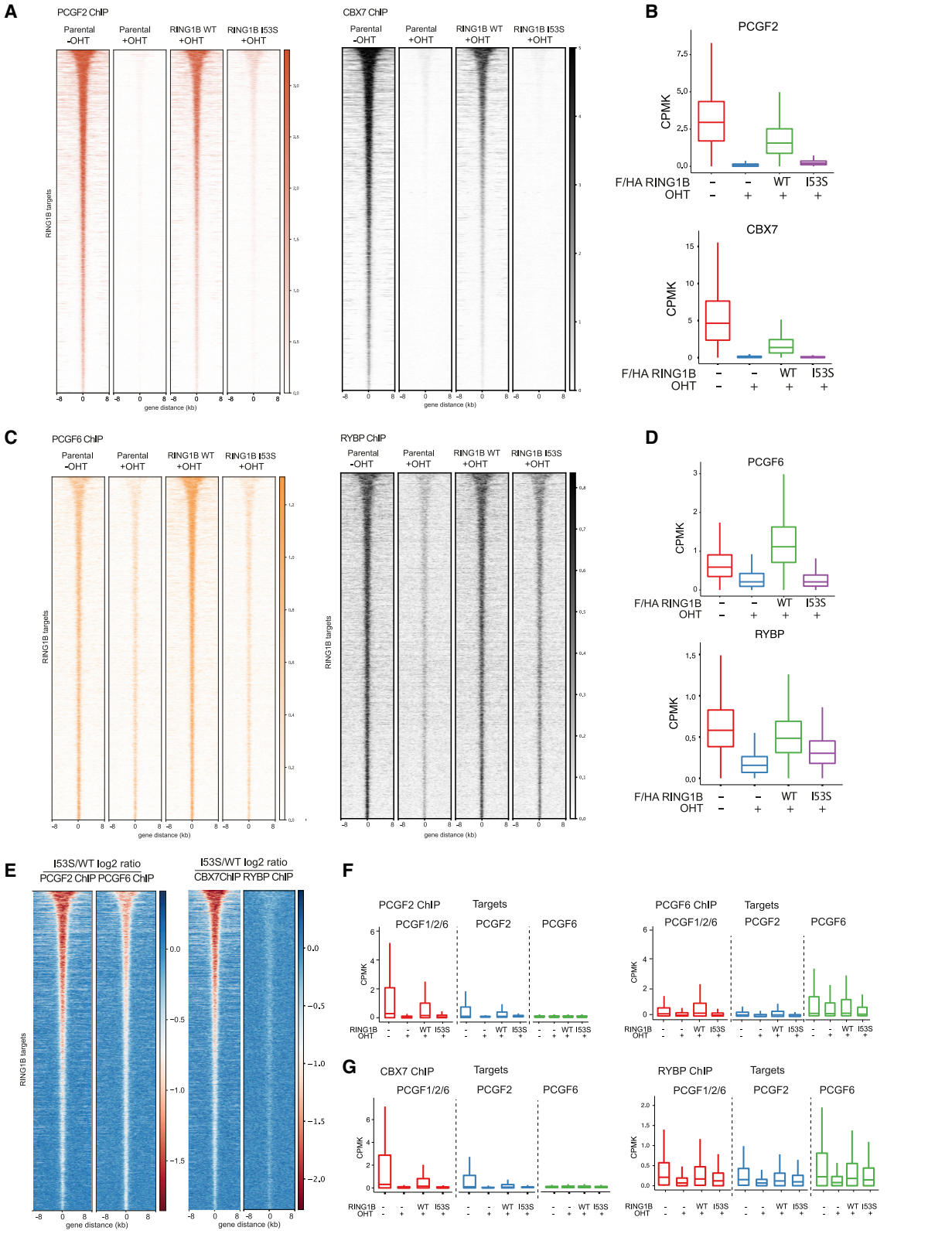

(legend on next page)

still observed in the absence of H2AK119ub1. Importantly, in the presence of H2AK119ub1 deposition, RING1B I53S was recruited to target loci with the same efficiency as its WT counterpart, demonstrating that its displacement was not an intrinsic DNA binding defect of this mutant. vPRC1 were also shown to retain *in vitro* affinity of H2AK119ub1 in ESC extracts (Kalb et al., 2014), suggesting a direct dependency on H2AK119ub1 deposition and a positive feedback loop mechanism that can further stabilize vPRC1 activity in addition to the PRC2-cPRC1 axis. Indeed, in the absence of H2AK119ub1 deposition, we observed a partial displacement of PCGF6, specifically at highly repressed sites. This observation further places H2AK119ub1 deposition in a central position to build up PcG repressive domains. This is consistent with the lack of transcriptional derepression reported for the acute deletion of PRC2 activity in ESCs (Riising et al., 2014) and further agrees with the lack of epistasis in early development and adult tissue homeostatic control between PRC1 and PRC2 activities (Chiacchiera et al., 2016a; Chiacchiera et al., 2016b).

Aberrant H2AK119ub1 deposition has also been linked to the development of several types of human cancers. This is specifically associated with the inactivation of the H2AK119ub1 specific de-ubiquitinase BAP1 that occurs with high frequency in uveal melanoma (~45%) and mesothelioma (~22%) as well as in several other tumor types with lower frequencies like atypical Spitz tumors (~11%), clear cell renal cell carcinoma (~18%), ovary (~5%), and colon-rectum (~3%) (Carbone et al., 2013). BAP1 inactivation always resulted in strong accumulation of H2AK119ub1 levels (Campagne et al., 2019) and, based on the canonical model by which PRC2 controls upstream PRC1 activity, it was proposed that BAP1-deficient tumors could benefit from PRC2 inhibition (LaFave et al., 2015). Our data argue against this possibility, placing H2AK119ub1 deposition in a central position to control PcG-mediated repression upstream to PRC2 and cPRC1 activities. This agrees with other reports that questioned the efficacy of PRC2 inhibition showing that viability of BAP1-deficient uveal melanoma cells is largely unaffected by PRC2 inhibition (Schoumacher et al., 2016). Based on our findings, we speculate that H2AK119ub1 deposition and vPRC1 activities could have a dominant role in controlling transcriptional repression also under pathological conditions with limited vulnerabilities within the PRC2-cPRC1 regulatory axis. Because we cannot exclude that BAP1 may also have additional roles that could be relevant in cancer progression (He et al., 2019), dissecting the contribution that vPRC1 forms play under pathological conditions of H2AK119ub1 deregulation will became a critical step for the future to define the tumor suppressive molecular properties of BAP1 and eventually uncover vulnerabilities for new strategies of intervention.

STAR★METHODS

Detailed methods are provided in the online version of this paper and include the following:

- KEY RESOURCES TABLE
- LEAD CONTACT AND MATERIALS AVAILABILITY
- EXPERIMENTAL MODEL AND SUBJECT DETAILS
  - Cell lines and cell culture
- METHOD DETAILS
  - Western Blot
  - Fractionation
  - Sample preparation and mass spectrometry analysis
  - Peptides and proteins identification
  - Quantitative real-time PCR (qPCR)
  - Chromatin immunoprecipitation (ChIP)
  - RNA-seq
  - ChIP-seq Analysis
  - RNA-seq Analysis
- DATA AND CODE AVAILABILITY

SUPPLEMENTAL INFORMATION

Supplemental Information can be found online at https://doi.org/10.1016/j.molcel.2019.11.021.

ACKNOWLEDGMENTS

We would like to acknowledge Federico Rossi for the help in analyzing mass spectrometry data, the IEO Genomic unit for support, and all members of the Pasini laboratory for helpful discussion. The work of the Pasini laboratory was supported by the Italian Association for Cancer Research (AIRC) (IG-2017-20290) and by the European Research Council (ERC) (EC-H2020-ERC-CoG-DissectPcG: 725268). D.F.-P. is a PhD student in the European School of Molecular Medicine (SEMM). D.M. was supported by a fellowship from FIRC and the European Institute of Oncology Foundation (FIEO). E.C. was supported by funding from AIRC and the European Union's Horizon 2020 research and innovation programme under the Marie Sklodowska-Curie grant agreement (800924).

AUTHOR CONTRIBUTIONS

S.T., E.L., and D.P. conceived the project. S.T. and E.L. performed the experimental work. D.F.-P. performed the computational analysis. D.M., M.Z., and E.C. provided support to the experimental work. S.T., E.L., and D.P. wrote the manuscript and edited the figures.

Figure 7. RING1B Inactivation Preferentially Affects cPRC1

(A) Heatmaps representing normalized PCGF2 and CBX7 ChIP-seq intensities ±8 kb around the center of RING1B target loci in the indicated cell lines.
(B) Boxplots representing PCGF2 ChIP-seq CPMK levels (top panel) and CBX7 (bottom panel) in the indicated cell lines at RING1B target loci.
(C) Heatmaps representing normalized PCGF6 and RYBP ChIP-seq intensities ±8 kb around the center of RING1B target loci in the indicated cell lines.
(D) Boxplots representing PCGF6 ChIP-seq CPMK levels (top panel) and RYBP (bottom panel) in the indicated cell lines at RING1B target loci.
(E) Heatmap representing the log2 ratio of PCGF2 and PCGF6 (left) and CBX7 and RYBP (right) normalized ChIP-seq intensities at RING1B target loci between RING1B WT- and I53S-expressing cells.
(F) Boxplots representing PCGF2 (upper panel) and PCGF6 (bottom panel) ChIP-seq CPMK levels ±250 bp around TSS of PCGF target genes in the indicated cell lines.
(G) Boxplots representing CBX7 (left panel) and RYBP (right panel) ChIP-seq CPMK levels ±250 bp around TSS of PCGF target genes in the indicated cell lines.
See also Figures S2A–S2C.

DECLARATIONS OF INTERESTS

The authors declare no competing interests.

Received: July 2, 2019
Revised: October 18, 2019
Accepted: November 26, 2019
Published: December 26, 2019

REFERENCES

Anders, S., Pyl, P.T., and Huber, W. (2015). HTSeq–a Python framework to work with high-throughput sequencing data. Bioinformatics *31*, 166–169.

Ben-Saadon, R., Zaaroor, D., Ziv, T., and Ciechanover, A. (2006). The polycomb protein Ring1B generates self atypical mixed ubiquitin chains required for its in vitro histone H2A ligase activity. Mol. Cell *24*, 701–711.

Beringer, M., Pisano, P., Di Carlo, V., Blanco, E., Chammas, P., Vizán, P., Gutiérrez, A., Aranda, S., Payer, B., Wierer, M., and Di Croce, L. (2016). EPOP Functionally Links Elongin and Polycomb in Pluripotent Stem Cells. Mol. Cell *64*, 645–658.

Bernstein, E., Duncan, E.M., Masui, O., Gil, J., Heard, E., and Allis, C.D. (2006). Mouse polycomb proteins bind differentially to methylated histone H3 and RNA and are enriched in facultative heterochromatin. Mol. Cell. Biol. *26*, 2560–2569.

Blackledge, N.P., Farcas, A.M., Kondo, T., King, H.W., McGouran, J.F., Hanssen, L.L., Ito, S., Cooper, S., Kondo, K., Koseki, Y., et al. (2014). Variant PRC1 complex-dependent H2A ubiquitylation drives PRC2 recruitment and polycomb domain formation. Cell *157*, 1445–1459.

Blackledge, N.P., Rose, N.R., and Klose, R.J. (2015). Targeting Polycomb systems to regulate gene expression: modifications to a complex story. Nat. Rev. Mol. Cell Biol. *16*, 643–649.

Blecher-Gonen, R., Barnett-Itzhaki, Z., Jaitin, D., Amann-Zalcenstein, D., Lara-Astiaso, D., and Amit, I. (2013). High-throughput chromatin immunoprecipitation for genome-wide mapping of in vivo protein-DNA interactions and epigenomic states. Nat. Protoc. *8*, 539–554.

Bracken, A.P., and Helin, K. (2009). Polycomb group proteins: navigators of lineage pathways led astray in cancer. Nat. Rev. Cancer *9*, 773–784.

Bracken, A.P., Pasini, D., Capra, M., Prosperini, E., Colli, E., and Helin, K. (2003). EZH2 is downstream of the pRB-E2F pathway, essential for proliferation and amplified in cancer. EMBO J. *22*, 5323–5335.

Buchwald, G., van der Stoop, P., Weichenrieder, O., Perrakis, A., van Lohuizen, M., and Sixma, T.K. (2006). Structure and E3-ligase activity of the Ring-Ring complex of polycomb proteins Bmi1 and Ring1b. EMBO J. *25*, 2465–2474.

Campagne, A., Lee, M.K., Zielinski, D., Michaud, A., Le Corre, S., Dingli, F., Chen, H., Shahidian, L.Z., Vassilev, I., Servant, N., et al. (2019). BAP1 complex promotes transcription by opposing PRC1-mediated H2A ubiquitylation. Nat. Commun. *10*, 348.

Cao, R., Wang, L., Wang, H., Xia, L., Erdjument-Bromage, H., Tempst, P., Jones, R.S., and Zhang, Y. (2002). Role of histone H3 lysine 27 methylation in Polycomb-group silencing. Science *298*, 1039–1043.

Carbone, M., Yang, H., Pass, H.I., Krausz, T., Testa, J.R., and Gaudino, G. (2013). BAP1 and cancer. Nat. Rev. Cancer *13*, 153–159.

Chan, H.L., and Morey, L. (2019). Emerging Roles for Polycomb-Group Proteins in Stem Cells and Cancer. Trends Biochem. Sci. *44*, 688–700.

Chen, H., and Boutros, P.C. (2011). VennDiagram: a package for the generation of highly-customizable Venn and Euler diagrams in R. BMC Bioinformatics *12*, 35.

Chiacchiera, F., and Pasini, D. (2017). Control of adult intestinal identity by the Polycomb repressive machinery. Cell Cycle *16*, 243–244.

Chiacchiera, F., Rossi, A., Jammula, S., Piunti, A., Scelfo, A., Ordóñez-Morán, P., Huelsken, J., Koseki, H., and Pasini, D. (2016a). Polycomb Complex PRC1 Preserves Intestinal Stem Cell Identity by Sustaining Wnt/β-Catenin Transcriptional Activity. Cell Stem Cell *18*, 91–103.

Chiacchiera, F., Rossi, A., Jammula, S., Zanotti, M., and Pasini, D. (2016b). PRC2 preserves intestinal progenitors and restricts secretory lineage commitment. EMBO J. *35*, 2301–2314.

Comet, I., Riising, E.M., Leblanc, B., and Helin, K. (2016). Maintaining cell identity: PRC2-mediated regulation of transcription and cancer. Nat. Rev. Cancer *16*, 803–810.

Conway, E., Jerman, E., Healy, E., Ito, S., Holoch, D., Oliviero, G., Deevy, O., Glancy, E., Fitzpatrick, D.J., Mucha, M., et al. (2018). A Family of Vertebrate-Specific Polycombs Encoded by the LCOR/LCORL Genes Balance PRC2 Subtype Activities. Mol. Cell *70*, 408–421.

Cooper, S., Grijzenhout, A., Underwood, E., Ancelin, K., Zhang, T., Nesterova, T.B., Anil-Kirmizitas, B., Bassett, A., Kooistra, S.M., Agger, K., et al. (2016). Jarid2 binds mono-ubiquitylated H2A lysine 119 to mediate crosstalk between Polycomb complexes PRC1 and PRC2. Nat. Commun. *7*, 13661.

Cox, J., and Mann, M. (2008). MaxQuant enables high peptide identification rates, individualized p.p.b.-range mass accuracies and proteome-wide protein quantification. Nat. Biotechnol. *26*, 1367–1372.

Elderkin, S., Maertens, G.N., Endoh, M., Mallery, D.L., Morrice, N., Koseki, H., Peters, G., Brockdorff, N., and Hiom, K. (2007). A phosphorylated form of Mel-18 targets the Ring1B histone H2A ubiquitin ligase to chromatin. Mol. Cell *28*, 107–120.

ENCODE Project Consortium (2012). An integrated encyclopedia of DNA elements in the human genome. Nature *489*, 57–74.

Endoh, M., Endo, T.A., Endoh, T., Fujimura, Y., Ohara, O., Toyoda, T., Otte, A.P., Okano, M., Brockdorff, N., Vidal, M., and Koseki, H. (2008). Polycomb group proteins Ring1A/B are functionally linked to the core transcriptional regulatory circuitry to maintain ES cell identity. Development *135*, 1513–1524.

Endoh, M., Endo, T.A., Endoh, T., Isono, K., Sharif, J., Ohara, O., Toyoda, T., Ito, T., Eskeland, R., Bickmore, W.A., et al. (2012). Histone H2A mono-ubiquitination is a crucial step to mediate PRC1-dependent repression of developmental genes to maintain ES cell identity. PLoS Genet. *8*, e1002774.

Farcas, A.M., Blackledge, N.P., Sudbery, I., Long, H.K., McGouran, J.F., Rose, N.R., Lee, S., Sims, D., Cerase, A., Sheahan, T.W., et al. (2012). KDM2B links the Polycomb Repressive Complex 1 (PRC1) to recognition of CpG islands. eLife *1*, e00205.

Faust, G.G., and Hall, I.M. (2014). SAMBLASTER: fast duplicate marking and structural variant read extraction. Bioinformatics *30*, 2503–2505.

Faust, C., Lawson, K.A., Schork, N.J., Thiel, B., and Magnuson, T. (1998). The Polycomb-group gene eed is required for normal morphogenetic movements during gastrulation in the mouse embryo. Development *125*, 4495–4506.

Ferrari, K.J., Scelfo, A., Jammula, S., Cuomo, A., Barozzi, I., Stützer, A., Fischle, W., Bonaldi, T., and Pasini, D. (2014). Polycomb-dependent H3K27me1 and H3K27me2 regulate active transcription and enhancer fidelity. Mol. Cell *53*, 49–62.

Flavahan, W.A., Gaskell, E., and Bernstein, B.E. (2017). Epigenetic plasticity and the hallmarks of cancer. Science *357*, eaal2380.

Fursova, N.A., Blackledge, N.P., Nakayama, M., Ito, S., Koseki, Y., Farcas, A.M., King, H.W., Koseki, H., and Klose, R.J. (2019). Synergy between Variant PRC1 Complexes Defines Polycomb-Mediated Gene Repression. Mol. Cell *74*, 1020–1036.

Gao, Z., Zhang, J., Bonasio, R., Strino, F., Sawai, A., Parisi, F., Kluger, Y., and Reinberg, D. (2012). PCGF homologs, CBX proteins, and RYBP define functionally distinct PRC1 family complexes. Mol. Cell *45*, 344–356.

Grijzenhout, A., Godwin, J., Koseki, H., Gdula, M.R., Szumska, D., McGouran, J.F., Bhattacharya, S., Kessler, B.M., Brockdorff, N., and Cooper, S. (2016). Functional analysis of AEBP2, a PRC2 Polycomb protein, reveals a Trithorax phenotype in embryonic development and in ESCs. Development *143*, 2716–2723.

Hauri, S., Comoglio, F., Seimiya, M., Gerstung, M., Glatter, T., Hansen, K., Aebersold, R., Paro, R., Gstaiger, M., and Beisel, C. (2016). A High-Density Map for Navigating the Human Polycomb Complexome. Cell Rep. *17*, 583–595.

He, M., Chaurushiya, M.S., Webster, J.D., Kummerfeld, S., Reja, R., Chaudhuri, S., Chen, Y.J., Modrusan, Z., Haley, B., Dugger, D.L., et al. (2019). Intrinsic apoptosis shapes the tumor spectrum linked to inactivation of the deubiquitinase BAP1. Science *364*, 283–285.

Healy, E., Mucha, M., Glancy, E., Fitzpatrick, D.J., Conway, E., Neikes, H.K., Monger, C., Van Mierlo, G., Baltissen, M.P., Koseki, Y., et al. (2019). PRC2.1 and PRC2.2 Synergize to Coordinate H3K27 Trimethylation. Mol. Cell *76*, 437–452.

Heinz, S., Benner, C., Spann, N., Bertolino, E., Lin, Y.C., Laslo, P., Cheng, J.X., Murre, C., Singh, H., and Glass, C.K. (2010). Simple combinations of lineage-determining transcription factors prime cis-regulatory elements required for macrophage and B cell identities. Mol. Cell *38*, 576–589.

Hojfeldt, J.W., Hedehus, L., Laugesen, A., Tatar, T., Wiehle, L., and Helin, K. (2019). Non-core Subunits of the PRC2 Complex Are Collectively Required for Its Target-Site Specificity. Mol. Cell *76*, 423–436.

Huang, Y., Zhao, W., Wang, C., Zhu, Y., Liu, M., Tong, H., Xia, Y., Jiang, Q., and Qin, J. (2018). Combinatorial Control of Recruitment of a Variant PRC1.6 Complex in Embryonic Stem Cells. Cell Rep. *22*, 3032–3043.

Ignatiadis, N., Klaus, B., Zaugg, J.B., and Huber, W. (2016). Data-driven hypothesis weighting increases detection power in genome-scale multiple testing. Nat. Methods *13*, 577–580.

Illingworth, R.S., Moffat, M., Mann, A.R., Read, D., Hunter, C.J., Pradeepa, M.M., Adams, I.R., and Bickmore, W.A. (2015). The E3 ubiquitin ligase activity of RING1B is not essential for early mouse development. Genes Dev. *29*, 1897–1902.

Jenuwein, T., and Allis, C.D. (2001). Translating the histone code. Science *293*, 1074–1080.

Kalb, R., Latwiel, S., Baymaz, H.I., Jansen, P.W., Müller, C.W., Vermeulen, M., and Müller, J. (2014). Histone H2A monoubiquitination promotes histone H3 methylation in Polycomb repression. Nat. Struct. Mol. Biol. *21*, 569–571.

Kundu, S., Ji, F., Sunwoo, H., Jain, G., Lee, J.T., Sadreyev, R.I., Dekker, J., and Kingston, R.E. (2017). Polycomb Repressive Complex 1 Generates Discrete Compacted Domains that Change during Differentiation. Mol. Cell *65*, 432–446.

LaFave, L.M., Béguelin, W., Koche, R., Teater, M., Spitzer, B., Chramiec, A., Papalexi, E., Keller, M.D., Hricik, T., Konstantinoff, K., et al. (2015). Loss of BAP1 function leads to EZH2-dependent transformation. Nat. Med. *21*, 1344–1349.

Langmead, B., Trapnell, C., Pop, M., and Salzberg, S.L. (2009). Ultrafast and memory-efficient alignment of short DNA sequences to the human genome. Genome Biol. *10*, R25.

Laugesen, A., Højfeldt, J.W., and Helin, K. (2019). Molecular Mechanisms Directing PRC2 Recruitment and H3K27 Methylation. Mol. Cell *74*, 8–18.

Lavarone, E., Barbieri, C.M., and Pasini, D. (2019). Dissecting the role of H3K27 acetylation and methylation in PRC2 mediated control of cellular identity. Nat. Commun. *10*, 1679.

Lee, C.H., Yu, J.R., Kumar, S., Jin, Y., LeRoy, G., Bhanu, N., Kaneko, S., Garcia, B.A., Hamilton, A.D., and Reinberg, D. (2018). Allosteric Activation Dictates PRC2 Activity Independent of Its Recruitment to Chromatin. Mol. Cell *70*, 422–434.

Liao, Y., Smyth, G.K., and Shi, W. (2014). featureCounts: an efficient general purpose program for assigning sequence reads to genomic features. Bioinformatics *30*, 923–930.

Love, M.I., Huber, W., and Anders, S. (2014). Moderated estimation of fold change and dispersion for RNA-seq data with DESeq2. Genome Biol. *15*, 550.

Margueron, R., and Reinberg, D. (2011). The Polycomb complex PRC2 and its mark in life. Nature *469*, 343–349.

Margueron, R., Li, G., Sarma, K., Blais, A., Zavadil, J., Woodcock, C.L., Dynlacht, B.D., and Reinberg, D. (2008). Ezh1 and Ezh2 maintain repressive chromatin through different mechanisms. Mol. Cell *32*, 503–518.

Margueron, R., Justin, N., Ohno, K., Sharpe, M.L., Son, J., Drury, W.J., 3rd, Voigt, P., Martin, S.R., Taylor, W.R., De Marco, V., et al. (2009). Role of the polycomb protein EED in the propagation of repressive histone marks. Nature *461*, 762–767.

Mendenhall, E.M., Koche, R.P., Truong, T., Zhou, V.W., Issac, B., Chi, A.S., Ku, M., and Bernstein, B.E. (2010). GC-rich sequence elements recruit PRC2 in mammalian ES cells. PLoS Genet. *6*, e1001244.

O'Carroll, D., Erhardt, S., Pagani, M., Barton, S.C., Surani, M.A., and Jenuwein, T. (2001). The polycomb-group gene Ezh2 is required for early mouse development. Mol. Cell. Biol. *21*, 4330–4336.

Oksuz, O., Narendra, V., Lee, C.H., Descostes, N., LeRoy, G., Raviram, R., Blumenberg, L., Karch, K., Rocha, P.P., Garcia, B.A., et al. (2018). Capturing the Onset of PRC2-Mediated Repressive Domain Formation. Mol. Cell *70*, 1149–1162.

Orlando, D.A., Chen, M.W., Brown, V.E., Solanki, S., Choi, Y.J., Olson, E.R., Fritz, C.C., Bradner, J.E., and Guenther, M.G. (2014). Quantitative ChIP-Seq normalization reveals global modulation of the epigenome. Cell Rep. *9*, 1163–1170.

Paro, R. (1990). Imprinting a determined state into the chromatin of Drosophila. Trends Genet. *6*, 416–421.

Pasini, D., and Di Croce, L. (2016). Emerging roles for Polycomb proteins in cancer. Curr. Opin. Genet. Dev. *36*, 50–58.

Pasini, D., Bracken, A.P., Jensen, M.R., Lazzerini Denchi, E., and Helin, K. (2004). Suz12 is essential for mouse development and for EZH2 histone methyltransferase activity. EMBO J. *23*, 4061–4071.

Pasini, D., Bracken, A.P., Hansen, J.B., Capillo, M., and Helin, K. (2007). The polycomb group protein Suz12 is required for embryonic stem cell differentiation. Mol. Cell. Biol. *27*, 3769–3779.

Pasini, D., Bracken, A.P., Agger, K., Christensen, J., Hansen, K., Cloos, P.A., and Helin, K. (2008). Regulation of stem cell differentiation by histone methyltransferases and demethylases. Cold Spring Harb. Symp. Quant. Biol. *73*, 253–263.

Pengelly, A.R., Copur, Ö., Jäckle, H., Herzig, A., and Müller, J. (2013). A histone mutant reproduces the phenotype caused by loss of histone-modifying factor Polycomb. Science *339*, 698–699.

Pengelly, A.R., Kalb, R., Finkl, K., and Müller, J. (2015). Transcriptional repression by PRC1 in the absence of H2A monoubiquitylation. Genes Dev. *29*, 1487–1492.

Picelli, S., Faridani, O.R., Björklund, A.K., Winberg, G., Sagasser, S., and Sandberg, R. (2014). Full-length RNA-seq from single cells using Smart-seq2. Nat. Protoc. *9*, 171–181.

Pivetti, S., Fernandez-Perez, D., D'Ambrosio, A., Barbieri, C.M., Manganaro, D., Rossi, A., Barnabei, L., Zanotti, M., Scelfo, A., Chiacchiera, F., et al. (2019). Loss of PRC1 activity in different stem cell compartments activates a common transcriptional program with cell type-dependent outcomes. Sci. Adv. *5*, eaav1594.

Posfai, E., Kunzmann, R., Brochard, V., Salvaing, J., Cabuy, E., Roloff, T.C., Liu, Z., Tardat, M., van Lohuizen, M., Vidal, M., et al. (2012). Polycomb function during oogenesis is required for mouse embryonic development. Genes Dev. *26*, 920–932.

Ramírez, F., Ryan, D.P., Grüning, B., Bhardwaj, V., Kilpert, F., Richter, A.S., Heyne, S., Dündar, F., and Manke, T. (2016). deepTools2: a next generation web server for deep-sequencing data analysis. Nucleic Acids Res. *44* (W1), W160-5.

Riising, E.M., Comet, I., Leblanc, B., Wu, X., Johansen, J.V., and Helin, K. (2014). Gene silencing triggers polycomb repressive complex 2 recruitment to CpG islands genome wide. Mol. Cell *55*, 347–360.

Rose, N.R., King, H.W., Blackledge, N.P., Fursova, N.A., Ember, K.J., Fischer, R., Kessler, B.M., and Klose, R.J. (2016). RYBP stimulates PRC1 to shape chromatin-based communication between Polycomb repressive complexes. eLife *5*, e18591.

Scelfo, A., Piunti, A., and Pasini, D. (2015). The controversial role of the Polycomb group proteins in transcription and cancer: how much do we not understand Polycomb proteins? FEBS J. *282*, 1703–1722.

Scelfo, A., Fernández-Pérez, D., Tamburri, S., Zanotti, M., Lavarone, E., Soldi, M., Bonaldi, T., Ferrari, K.J., and Pasini, D. (2019). Functional Landscape of PCGF Proteins Reveals Both RING1A/B-Dependent-and RING1A/B-Independent-Specific Activities. Mol. Cell *74*, 1037–1052.

Schoumacher, M., Le Corre, S., Houy, A., Mulugeta, E., Stern, M.H., Roman-Roman, S., and Margueron, R. (2016). Uveal melanoma cells are resistant to EZH2 inhibition regardless of BAP1 status. Nat. Med. *22*, 577–578.

Shen, X., Liu, Y., Hsu, Y.J., Fujiwara, Y., Kim, J., Mao, X., Yuan, G.C., and Orkin, S.H. (2008). EZH1 mediates methylation on histone H3 lysine 27 and complements EZH2 in maintaining stem cell identity and executing pluripotency. Mol. Cell *32*, 491–502.

Stielow, B., Finkernagel, F., Stiewe, T., Nist, A., and Suske, G. (2018). MGA, L3MBTL2 and E2F6 determine genomic binding of the non-canonical Polycomb repressive complex PRC1.6. PLoS Genet. *14*, e1007193.

Tavares, L., Dimitrova, E., Oxley, D., Webster, J., Poot, R., Demmers, J., Bezstarosti, K., Taylor, S., Ura, H., Koide, H., et al. (2012). RYBP-PRC1 complexes mediate H2A ubiquitylation at polycomb target sites independently of PRC2 and H3K27me3. Cell *148*, 664–678.

Trapnell, C., Pachter, L., and Salzberg, S.L. (2009). TopHat: discovering splice junctions with RNA-Seq. Bioinformatics *25*, 1105–1111.

Tsuboi, M., Kishi, Y., Yokozeki, W., Koseki, H., Hirabayashi, Y., and Gotoh, Y. (2018). Ubiquitination-Independent Repression of PRC1 Targets during Neuronal Fate Restriction in the Developing Mouse Neocortex. Dev. Cell *47*, 758–772.

Wang, H., Wang, L., Erdjument-Bromage, H., Vidal, M., Tempst, P., Jones, R.S., and Zhang, Y. (2004). Role of histone H2A ubiquitination in Polycomb silencing. Nature *431*, 873–878.

Yu, X., and Cheng, Y. (2019). Data-driven Q-matrix validation using a residual-based statistic in cognitive diagnostic assessment. Br. J. Math. Stat. Psychol. Published online November 25, 2019. https://doi.org/10.1111/bmsp.12191.

Zhang, Y., Liu, T., Meyer, C.A., Eeckhoute, J., Johnson, D.S., Bernstein, B.E., Nusbaum, C., Myers, R.M., Brown, M., Li, W., and Liu, X.S. (2008). Model-based analysis of ChIP-Seq (MACS). Genome Biol. *9*, R137.

Zhu, L.J., Gazin, C., Lawson, N.D., Pagès, H., Lin, S.M., Lapointe, D.S., and Green, M.R. (2010). ChIPpeakAnno: a Bioconductor package to annotate ChIP-seq and ChIP-chip data. BMC Bioinformatics *11*, 237.

Zhu, A., Ibrahim, J.G., and Love, M.I. (2019). Heavy-tailed prior distributions for sequence count data: removing the noise and preserving large differences. Bioinformatics *35*, 2084–2092.

STAR★METHODS

KEY RESOURCES TABLE

REAGENT or RESOURCE	SOURCE	IDENTIFIER
Antibodies		
Rabbit polyclonal anti-Pcgf1	Scelfo et al., 2019	N/A
Rabbit polyclonal anti-Pcgf2	Scelfo et al., 2019	N/A
Rabbit polyclonal anti-Pcgf6	Scelfo et al., 2019	N/A
Rabbit polyclonal anti-Ring1b	Chiacchiera et al., 2016a	N/A
Mouse monoclonal anti-Vinculin	Merck (Sigma Aldrich)	Cat# V9131; RRID: AB_477629
Rabbit polyclonal anti-DEDAF (RYBP)	Merck (Sigma Aldrich)	Cat# AB3637; RRID: AB_2285466
Rabbit polyclonal anti-Cbx7	Abcam	Cat# ab21873; RRID: AB_726005
Rabbit monoclonal anti-Suz12 (D39F6)	Cell Signaling Technology	Cat# 3737; RRID: AB_2196850
Rabbit monoclonal anti-tri-methyl-histone H3 (Lys27) (C36B11)	Cell Signaling Technology	Cat# 9733; RRID: AB_2616029
Rabbit monoclonal anti-ubiquityl histone H2A (Lys119) (D27C4)	Cell Signaling Technology	Cat# 8240; RRID: AB_10891618
Rabbit monoclonal anti-Bap1 (D7W70)	Cell Signaling Technology	Cat# 13271; RRID: AB_2798168
Mouse monoclonal anti-H3K27me1	Active Motif	Cat# 61015; RRID: AB_2715573
Rabbit monoclonal anti-di-methyl-histone H3 (Lys27) (D18C8)	Cell Signaling Technology	Cat# 9728; RRID: AB_1281338
Mouse monoclonal anti-Eed	Bracken et al., 2003	N/A
Mouse monoclonal anti-Ezh2	Pasini et al., 2004	N/A
Rabbit monoclonal anti-histone H3	Abcam	Cat# ab1791; RRID: AB_302613
Rabbit polyclonal anti-histone H2A (acidic patch)	Merck (Sigma Aldrich)	Cat# 07-146; RRID: AB_310394
Rabbit polyclonal anti-Mtf2	Proteintech	Cat# 16208-1-AP; RRID: AB_2147370
Rabbit monoclonal anti-Jarid2 (D6M9X)	Cell Signaling Technology	Cat# 13594; RRID: AB_2798269
Goat polyclonal anti-Lamin B (M-20)	Santa Cruz Biotechnology	Cat# sc-6217; RRID: AB_648158
Rabbit polyclonal anti-C17orf96 (EPOP)	Active Motif	Cat# 61753; RRID: AB_2793758
Rabbit monoclonal anti-AEBP2 (D7C6X)	Cell Signaling Technology	Cat# 14129; RRID: AB_2798398
Rabbit monoclonal anti-HA (12CA5)	Pasini laboratory	N/A
Goat polyclonal anti-Suz12 (P-15)	Santa Cruz Biotechnology	Cat# sc-46264; RRID: AB_2196857
Mouse monoclonal anti-Actin (AC-40)	Merck (Sigma Aldrich)	Cat# A3853; RRID: AB_262137
Rabbit IgG Control Antibody	Merck (Sigma Aldrich)	Cat# I5006; RRID: AB_1163659
Anti-FLAG M2 affinity gel	Merck (Sigma Aldrich)	Cat# A2220; RRID: AB_10063035
Bacterial and Virus Strains		
One Shot™ TOP10 Chemically Competent *E. coli*	Thermo Fisher Scientific (Invitrogen)	Cat# C404010
One Shot™ Stbl3™ Chemically Competent *E. coli*	Thermo Fisher Scientific (Invitrogen)	Cat# C737303
One Shot™ BL21(DE3) Chemically Competent *E. coli*	Thermo Fisher Scientific (Invitrogen)	Cat# C600003
Chemicals, Peptides, and Recombinant Proteins		
Leukemia Inhibitory Factor	Pasini laboratory	N/A
CHIR-99021	Aurogen	Cat# S1263
PD-0325901	Aurogen	Cat# S1036
Lipofectamine 2000 Transfection Reagent	Thermo Fisher Scientific (Invitrogen)	Cat# 11668027
IGEPAL CA-630	Merck (Sigma Aldrich)	Cat# I8896

(*Continued on next page*)

Continued

REAGENT or RESOURCE	SOURCE	IDENTIFIER
3X FLAG Peptide	Merck (Millipore)	Cat# F4799
Ethylene glycol-bis(succinic acid N-hydroxysuccinimide ester)	Merck (Sigma Aldrich)	Cat# E3257
Critical Commercial Assays		
Agilent High Sensitivity DNA kit	Agilent	Cat# 5067-4626
QIAquick PCR purification kit	Qiagen	Cat# 28104
Quick-RNA™ MiniPrep extraction kit	Zymo Research	Cat# R1055
Deposited Data		
Raw files	This paper	GEO: GSE134053
Mouse reference genome NCBI build 38, GRCm38	Genome Reference Consortium	https://www.ncbi.nlm.nih.gov/grc/mouse
Drosophila reference genome Release 6 plus ISO1 mitochondrial genome	The FlyBase Consortium/ Berkeley *Drosophila* Genome Project/ Celera Genomics	https://www.ncbi.nlm.nih.gov/assembly/GCF_000001215.4/
Western Blot	This paper	https://doi.org/10.17632/x6k27wtknb.2
Experimental Models: Cell Lines		
Mouse: Parental: ES cell line ROSA26:creERT2 RING1A-/-; RING1Bfl/fl	Endoh et al., 2008	N/A Strain of origin 129P2/Ola
Mouse: ES cell line E14	Pasini laboratory	N/A Strain of origin 129P2/Ola
Mouse: RING1B WT: ES cell line ROSA26:creERT2 RING1A-/-; RING1Bfl/fl; RING1B WT	This paper	N/A Strain of origin 129P2/Ola
Mouse: RING1B 153S: ES cell line ROSA26:creERT2 RING1A-/-; RING1Bfl/fl; RING1B I53S	This paper	N/A Strain of origin 129P2/Ola
Mouse: EED fl/fl clone#1: ES cell line ROSA26:creERT2 EED fl/fl	This paper	N/A Strain of origin 129P2/Ola
Mouse: EED fl/fl clone#4: ES cell line ROSA26:creERT2 EED fl/fl	This paper	N/A Strain of origin 129P2/Ola
Mouse: Parental MTF2 KO: ES cell line ROSA26:creERT2 RING1A-/-; RING1Bfl/fl; MTF2-/-	This paper	N/A Strain of origin 129P2/Ola
Mouse: RING1B WT MTF2 KO: ES cell line ROSA26:creERT2 RING1A-/-; RING1Bfl/fl; RING1B WT; MTF2-/-	This paper	N/A Strain of origin 129P2/Ola
Mouse: RING1B I53S MTF2 KO: ES cell line ROSA26:creERT2 RING1A-/-; RING1Bfl/fl; RING1B I53S; MTF2-/-	This paper	N/A Strain of origin 129P2/Ola
Mouse: Ezh2 KO Ezh1 KO: ES cell line EZH2-/-;EZH1-/-	Lavarone et al., 2019	N/A Strain of origin 129P2/Ola
Drosophila S2 cell line	ATCC	ATCC CRL- 1963
Oligonucleotides		
gRNA targeting Mtf2 exon 4 Forward: CACCGATGGTTATATGTGATAAGTG	This paper	N/A
gRNA targeting Mtf2 exon 4 Reverse: AAACCACTTATCACATATAACCATC	This paper	N/A
gRNA targeting Mtf2 exon 15 Forward: CACCGCCTCTTCTTCTCCGCAAATG	This paper	N/A
gRNA targeting Mtf2 exon 15 Reverse: AAACCATTTGCGGAGAAGAAGAGGC	This paper	N/A

(*Continued on next page*)

Continued

REAGENT or RESOURCE	SOURCE	IDENTIFIER
Recombinant DNA		
Plasmid: pSpCas9(BB)-2A-GFP (PX458)	Zhang Laboratory	Addgene plasmid #48138
Plasmid: pCAG 2XFLAG-HA	Pasini laboratory	N/A
Software and Algorithms		
Bowtie v1.2.2	Langmead et al., 2009	http://bowtie-bio.sourceforge.net/index.shtml
PICARD	N/A	http://broadinstitute.github.io/picard
MACS2 v2.1.1	Zhang et al., 2008	https://github.com/taoliu/MACS
ChIPpeakAnno v3.15	Zhu et al., 2010	Zhu et al., 2010
VennDiagram v1.6.20	Chen and Boutros, 2011	https://www.rdocumentation.org/packages/VennDiagram
ClusterProfiler	Yu and Cheng, 2019	http://bioconductor.org/packages/release/bioc/html/clusterProfiler.html
HOMER	Heinz et al., 2010	http://homer.ucsd.edu/
DeepTools 2.0	Ramírez et al., 2016	https://deeptools.readthedocs.io/en/latest/
STAR v2.7	N/A	N/A
DESeq2 v1.20	Love et al., 2014	N/A
TopHat v2.1.1	Trapnell et al., 2009	https://ccb.jhu.edu/software/tophat/
HTseq-count v0.8.0	Anders et al., 2015	http://www-huber.embl.de/HTSeq
MaxQuant software (version 1.5.2.8)	Cox and Mann, 2008	https://maxquant.org

LEAD CONTACT AND MATERIALS AVAILABILITY

Further information and requests for resources and reagents should be directed to and will be fulfilled by the lead contact, Diego Pasini (diego.pasini@ieo.it).

EXPERIMENTAL MODEL AND SUBJECT DETAILS

Cell lines and cell culture

ROSA26::creERT2 RING1A−/−; RING1Bfl/fl conditional mESC (Endoh et al., 2008) were engineered in order to stably express wild-type or I53A/S RING1B. mESCs were grown on 0.1% gelatin-coated dishes in 2i/LIF-containing GMEM medium (Euroclone) supplemented with 20% fetal calf serum (Euroclone), 2 mM glutamine (GIBCO), 100 U/ml penicillin, 0.1 mg/ml streptomycin (GIBCO), 0.1 mM non-essential amino acids (GIBCO), 1 mM sodium pyruvate (GIBCO), 50 μM β-mercaptoethanol phosphate buffered saline (PBS; GIBCO), 1000 U/ml leukemia inhibitory factor (LIF; produced in-house), and GSK3β and MEK 1/2 inhibitors (ABCR GmbH) to a final concentration of 3 μM and 1 μM, respectively. Indicated cells were treated for 48 or 72 h with 0.5 μM 4-hydroxytamoxifen (OHT; or EtOH as vehicle) in order to delete Ring1b gene. To generate stable MTF2 KO cell lines, 10 μg pX458 2.0 plasmids (Addgene) encoding Cas9 and sgRNAs were transfected using Lipofectamine 2000 (Invitrogen), according to the manufacturer's instruction. Sorting of GFP positive cells was carried-out 30 hr after transfection and 5000 cells were seeded into a 15-cm dish, and clones were isolated 10 days later. Clones were screened by Western Blot for protein lysates. PCR from positive clones were Sanger-sequenced to confirm genome editing.

The following gRNA guides were used for targeting: *Mtf2* Exon 4 CACCGATGGTTATATGTGATAAGTG and AAACCACTTATCACATATAACCATC; *Mtf2* Exon 15 CACCGCCTCTTCTTCTCCGCAAATG and AAACCATTTGCGGAGAAGAAGAGGC.

Eed conditional mESC were generated from blastocysts derived from ROSA26:creERT2 *Eed*$^{fl/fl}$ mice (Chiacchiera et al., 2016b) grown on 0.1% gelatin in the above described ESC medium.

For stable clones generation, ROSA26:creERT2 RING1A$^{-/-}$; RING1B$^{fl/fl}$ conditional mESCs were transfected with pCAG vectors encoding 2xFlag-HA-tagged mouse wild-type or RING1B I53A/S using Lipofectamine 2000 (ThermoFisher Scientific), according to manufacturer's instructions. Transfected cells were sub-cloned under puromycin selection (2 μg/ml) until the appearance of clones at day 10-12. Clones were screened by Western Blot and then selected for further analyses.

METHOD DETAILS

Western Blot

For western blot analysis on total protein lysates, mESCs were lysed and sonicated in ice-cold S300 buffer (20 mM Tris-HCl pH 8.0, 300 mM NaCl, 10% glycerol, 0.2% NP40) and supplemented with protease inhibitors (Roche). Nuclear extracts were obtained as described below. Briefly, cells were resuspended in Hypotonic Buffer (10 mM TrisHCl pH 7.6, 10mM KCl, 1.5 mM MgCl2 and 0,340 M Sucrose supplemented with 2 μg/mL Aprotinin, 1 μg/mL Leupeptin,) for 15 minutes at 4° (C). Then 0.3% of 10% Triton X-100 was added to the solution and vortexed for 30 s followed by high speed centrifugation. The nuclear pellet was then washed with hypotonic buffer and solubilized in S300 buffer. Co-immunoprecipitations were performed on 2 mg nuclear extracts using M2 agarose beads (30 μL slurry for IP, A2220 Anti-FLAG M2 affinity gel) for 2 hours at 4°(C). Immunocomplexes were washed 5 × with S300 buffer and eluted by competition with 1x Flag peptide (500 ng/ul; SIGMA) 2 times for 30 min at 16°C and then resuspended in Laemmli sample buffer. Protein lysates were separated on SDS-PAGE gels and transferred to nitrocellulose membranes. After probing with the suitable primary and secondary antibodies, chemoluminescence signals were captured with the ChemiDoc Imaging System (Bio-Rad).

Fractionation

Cellular pellets were lysed in 300 μL pre-extraction buffer (20mM HEPES pH 7.5, 0.5% Triton X-100, 50mM NaCl, 3mM MgCl2, 300mM Sucrose, 2 μg/mL Aprotinin, 1 μg/mL Leupeptin, 1mM PMSF) and incubated at 4°C for 30 minutes. 150 μL of suspension was removed and labeled "Total extract." The remaining lysate suspension was clarified at 13,000RPM in a 4°C centrifuge for 10 minutes. Supernatant was transferred to a new tube and labeled "Soluble fraction." The insoluble pellet was washed once in 1mL of pre-extraction buffer before resuspension in 150 μL of pre-extraction buffer. All samples were boiled at 99°C for 5 min before sonicating 10 times (30 s on, 30 s off) at high intensity on a diagenode water bath sonicator.

Sample preparation and mass spectrometry analysis

Proteins from RING1B WT and RING1B I53S purifications were separated for 2 cm by SDS–PAGE, using 4%–12% NuPAGE Novex Bis–Tris gels (Invitrogen)and NuPAGE MES SDS running buffer (Invitrogen) and then stained with Coomassie Blue using InstantBlue Comassie (Expedeon). Single bands from gel were cut and digested with trypsin (Promega) and incubated overnight at 37°C for protein digestion. Then, peptide extraction was carried out and the resulting peptides mixture were combined, desalted and concentrated using StageTip (Proxeon Biosystems) columns, washed with 30mL of 0,1% Formic acid (FA) and finally eluted with 40μL of 80% MeCN in 0,1% FA. The samples were concentrated in vacuum concentrator (Eppendorf concentrator 5301) and peptides were dissolved in 7μL of 0,1% FA. Approximately 6 μL of purified peptide mixture were analyzed on a LC–ESI–MS-MS Q-Exactive HF hybrid quadrupole-Orbitrap mass spectrometer (Thermo Fisher Scientific), using a gradient of 80 minutes with a flow of 250 nL/min. Full scan MS spectra were acquired in arange of m/z 300–1650.

Peptides and proteins identification

Raw data files were analyzed with MaxQuant software (version 1.5.2.8) using default parameters and performing searches against the Uniprot mouse ID:UP000000589 (released in 2019) as protein database. Additional parameters were match-between-runs, label-free quantification (LFQ) and IBAQ. The intensity of each hit in ETA, I53S_OHT and WT_OHT was normalized by the total sum of the intensity of all the hits and the average was calculated across the two replicas (ETA and ETA2, I53S_OHT and I53S_OHT2, WT_OHT and WT_OHT2). The normalized average intensity of each hit of interest in I53S and WT was divided by the corresponding value in ETA and the log2 of this ratio was reported in the heatmap (Figure 1E).

Quantitative real-time PCR (qPCR)

Total RNA was extracted with the Quick-RNA MiniPrep extraction kit (Zymo Research) and retro-transcribed with ImProm-II Reverse Transcription System (Promega) according to the manufacturer's instructions. Quantitative real-time PCR (qPCR) was carried out using GoTaq qPCR master mix (Promega) on CFX96 Real-Time PCR Detection System (Bio-Rad). Primer sequences are available upon request.

Chromatin immunoprecipitation (ChIP)

ChIP experiments were performed according to standard protocols as described previously (Ferrari et al., 2014). For SUZ12, RING1B, PCGF1, PCGF6, EPOP, JARID2, MTF2, RYBP,CBX7, AEBP2 and HA ChIPs, 1% formaldehyde cross-linked chromatin was sheared to 500–1000 bp fragments by sonication and incubated overnight in IP buffer (33 mM Tris-HCl pH 8, 100 mM NaCl, 5 mM EDTA, 0.2% NaN3, 0.33% SDS, 1.66% Triton X-100) at 4°C with the indicated antibodies (10 μg antibodies/ 500 μg chromatin). For histone modifications ChIPs, 250 μg of chromatin supplemented with 5% spike-in of S2 *Drosophila* chromatin (prepared in the same manner) and 5 μg of antibodies were used. The next day, chromatin lysates were incubated for 4 hours with protein-G Sepharose beads (GE Healthcare). Beads were washed 3 × with low-salt buffer (150 mM NaCl, 20 mM Tris-HCl pH 8, 2 mM EDTA, 0.1% SDS, 1% Triton X-100) and 1 × with high-salt buffer (500 mM NaCl, 20 mM Tris-HCl pH 8, 2 mM EDTA, 0.1% SDS, 1% Triton X-100), and then re-suspended in de-crosslinking solution (0.1 M NaHCO3, 1% SDS). DNA was purified with QIAquick PCR purification kit

(QIAGEN) according to manufacturer's instructions. DNA libraries were prepared with 2–10 ng of DNA using an in-house protocol (Blecher-Gonen et al., 2013) by the IEO genomic facility and sequenced on an Illumina HiSeq 2000.

RNA-seq

RNA-seq was performed following SMART-seq2 protocol (Picelli et al., 2014) with minor modifications. Briefly, poly-A containing mRNA molecules obtained from 1 μg of total RNA were copied into first-strand cDNA by reverse transcription and template-switching using oligo (dT) primers and an LNA-containing template-switching oligo (TSO). Resulting cDNA was pre-amplified with KAPA HotStart Taq enzyme (Kapa Biosystems) and then purified with Ampure beads (Agencourt AMPure XP- Beckman Coulter). Two nanograms of pre-amplified cDNA were tagmented with in-house produced Tn5 transposase and further amplified with KAPA HotStart Taq enzyme. After purification with Ampure beads, the quality of the obtained library was assessed by Bioanalyzer (High Sensitivity DNA kit, Agilent Technologies), prior to sequencing.

ChIP-seq Analysis

Paired-end reads were aligned to the mouse reference genome mm10, or mm10 and dm6 for histone ChIP-Rx, using Bowtie v1.2.2 (Langmead et al., 2009) without allowing for multi-mapping (–m 1) and parameters -I 10 -X 1000. PCR duplicates were removed using samblaster (Faust and Hall, 2014). Ambiguous reads mapping to both mm10 and dm6 were discarded. Peaks were called using MACS2 v2.1.1 (Zhang et al., 2008) with parameters -f BAMPE–keep-dup all -m 10 30 -p 1e-10. A list containing the final RING1B and H2AK119Ub1 peaks used in the analyses, called in the WT +OHT cell line, can be found in Table S2. Genomic peak annotation was performed with the R package ChIPpeakAnno v3.15 (Zhu et al., 2010), considering the region ± 2.5 kb around the center of the peak. PCGF target regions were obtain from Scelfo et al. (2019) and liftOver to mm10. Peak lists were then transformed to gene target lists, and overlaps were performed using the R package VennDiagram v1.6.20 (Chen and Boutros, 2011).

For heatmap and intensity plot representation of ChIP-seq signal, BigWig files with input signal subtracted were generated using the function bamCompare from deepTools 3.1 (Ramírez et al., 2016) with parameters–ratio subtract –bs 50–extendReads. To normalize for differences in sample library size, a scaling factor for each sample was calculated as (1/total mapped reads)*1000000 and was applied during BigWig file generation with the parameter–scaleFactors from bamCompare. For ChIP-Rx samples the scaling factor was calculated as described in Orlando et al. (2014). For the spike-in samples, a second scaling factor was calculated based on the ratio mm10/dm6 reads of the input samples (one per cell line). The scaling factor from a particular input is applied to all its respective ChIP-Rx samples. This allows to correct any potential difference in the amount of spike-in added to the different pools of chromatin, which was one per cell line. Heatmaps were performed using the functions computeMatrix with settings reference-point–referencePoint center/TSS -b 8000 -a 8000 -bs 50, followed by plotHeatmap from deepTools excluding blacklisted regions by ENCODE Project Consortium (2012). For boxplot representation, the function multiBigwigSummary (using BED-file and–outRawCounts options) from deeptools was used to calculate the average number of reads under peaks.

RNA-seq Analysis

Reads were aligned to the mouse reference genome mm10 using STAR v2.7 without allowing multimapping reads (–outFilterMultimapNmax 1). PCR duplicates were removed using samblaster (Faust and Hall, 2014). Gene counts were calculated using featureCounts (Liao et al., 2014) with parameters -s 0 -t exon -g gene_name using Gencode M21 (GRCm38) annotation downloaded from (https://www.gencodegenes.org/mouse/). Differential expression analyses were performed using the R package DESeq2 v1.20 (Love et al., 2014) using default parameters. Log2FoldChanges and adjusted p values were corrected using the apeglm (Zhu et al., 2019) and IHW (Ignatiadis et al., 2016) packages, respectively. Genes with an absolute log2 fold change of 1.5 and FDR < 0.05 were considered as differentially expressed (Table S3).

DATA AND CODE AVAILABILITY

The raw sequence data reported in this paper have been deposited in the NCBI Gene Expression Omnibus (GEO) with the accession number GEO: GSE134053.